Appendix D

NUMERICAL SIMULATION OF WEATHER AND CLIMATE

Technical Report No. 6

NSR-05-007-328

A SIMPLIFIED SCHEME FOR COMPUTING RADIATION TRANSFER IN THE TROPOSPHERE

DRA

by

A. Katayama

1973

Department of Meteorology

University of California, Los Angeles

ABSTRACT

A simplified scheme is presented, for the heating of clear and cloudy air by solar and infrared radiation transfer, designed for use in tropospheric general circulation models with coarse vertical resolution.

A bulk transmission function is defined for the infrared transfer. The interpolation factors, required for computing the bulk transmission function, are parameterized as functions of such physical parameters as the thickness of the layer, the pressure, and the mixing ratio at a reference level.

The computation procedure for solar radiation is significantly simplified by the introduction of two basic concepts. The first is that the solar radiation spectrum can be divided into a scattered part, for which Rayleigh scattering is significant but absorption by water vapor is negligible, and an absorbed part for which absorption by water vapor is significant but Rayleigh scattering is negligible. The second concept is that of an equivalent cloud water vapor amount which absorbs the same amount of radiation as the cloud.

Insert 1, p. II-2

$u^*_{H_2O}(z)$, is given by

$$u^*_{H_2O} = \frac{1}{g} \int_{p(z)}^{p_g} q_{H_2O} \left(\frac{p}{p_{oo}}\right)^{\alpha_{H_2O}} dp \qquad (II.3)$$

where q_{H_2O} is the mixing ratio of water vapor. A similar expression for the effective carbon dioxide amount is given by equation (IV.17).

Insert 2, p. II-2

Following Yamamoto (1952), the total transmission function of a mixture of water vapor and carbon dioxide is assumed to be represented by the product of their respective transmission functions, that is

$$\tau(u^*, T) = \tau_{H_2O}(u^*_{H_2O}, T)\ \tau_{CO_2}(u^*_{CO_2}, T)$$

and

$$\tilde{\tau}(u^*, T) = \tilde{\tau}_{H_2O}(u^*_{H_2O}, T)\ \tau_{CO_2}(u^*_{CO_2}, T)$$

As discussed in section 3(ii), $\tau_{CO_2}(u^*_{CO_2}, T)$ is assumed to be constant between any two isobaric levels. Thus τ and $\tilde{\tau}$ vary only with τ_{H_2O} and $\tilde{\tau}_{H_2O}$, respectively. Consequently, unless required for clarity, the subscript H_2O will henceforth be dropped from τ_{H_2O} and $\tilde{\tau}_{H_2O}$.

Insert 3, p. II-9

Experiments have been conducted with the GCM to determine, once and for all, the functional dependence expressed by equation (II.22). In these experiments, the integrals appearing in (II.16) and (II.17) were evaluated numerically by dividing the GCM layer under consideration into thin sublayers of 10 mb thickness. In this way,...

Insert 4, p. II-15

Following Yamamoto (1952), the total transmission function of a mixture of water vapor and carbon dioxide is assumed to be represented by the product of their respective transmission functions, that is

$$\tau(u^*_{H_2O}, u^*_{CO_2}, T) = \tau_{H_2O}(u^*_{H_2O}, T)\ \tau_{CO_2}(u^*_{CO_2}, T)$$

and

$$\tilde{\tau}(u^*_{H_2O}, u^*_{CO_2}, T) = \tilde{\tau}_{H_2O}(u^*_{H_2O}, T)\ \tau_{CO_2}(u^*_{CO_2}, T)$$

Yamamoto presents values of τ_{H_2O}, $\tilde{\tau}_{H_2O}$ and τ_{CO_2} (denoted in Tables II-2 to II-5 by Obs.) that are based upon experimental laboratory measurements of a generalized absorption coefficient in certain discrete spectral ranges. Using this experimental data, we deduce the following empirical equations for the transmission functions of water vapor and carbon dioxide.

Insert 5, p. IV-1

The effective water vapor amount in an air column of height z, $u^*(z)$, can be obtained from equation (II.3) if the continuous vertical distribution of water vapor mixing ratio q is known. Since the UCLA 3-layer GCM predicts q from the moisture conservation equation only at discrete levels, some approximation technique must be employed for equation (II.3). Smith (1966) has shown that the seasonal and latitudinal northern hemisphere mean value of the mixing ratio in the lower troposphere can be expressed by

$$q = q_o \left(\frac{p}{p_o}\right)^k , \qquad (IV.1)$$

where q_o is a known value of the mixing ratio at some pressure p_o. Utilizing different forms of this relation, in conjunction with the values of q predicted by the GCM, two methods for the evaluation of u^* will be developed subsequently.

TABLE OF CONTENTS

LIST OF FIGURES

LIST OF TABLES

1. INTRODUCTION

To accurately compute the fluxes of long wave radiation and solar ~~insolation~~ radiation in the atmosphere, it is necessary to discretize the spectrum and apply the equation of radiative transfer to each narrow wavelength interval. Furthermore, the atmosphere must be divided into a large number of thin layers for ~~the~~ an accurate computation, even when the general circulation model (GCM) has only a few layers. The amount of computer time required to calculate the radiative fluxes throughout the ~~entire~~ global atmosphere by this method is enormous and would exceed the combined time required for all the other computations of the GCM ~~combined~~. Consequently, it is desirable to have a simplified radiation computation scheme for ~~use with~~ a GCM ~~having~~ with coarse vertical resolution.

The ~~cloud system~~ clouds of the atmosphere strongly influence the radiational heating field. When the sky is covered by a dense cloud layer, the net flux of long wave radiation in the cloud layer is zero and ~~The~~ the top and bottom of the cloud layer are ~~treated as~~ black body radiators at their respective temperatures. The cooling due to long wave radiation is therefore significantly modified throughout the atmospheric column containing the cloud layer. Furthermore, ~~since~~ because a substantial fraction of the incident solar radiation is reflected or absorbed by a cloud layer, the vertical distribution of the heating ~~due to~~ by solar radiation is ~~largely~~ considerably affected by the cloud layer.

The radiative heating of clean and cloudy air is very complicated and at present we do not have a simple and accurate calculation scheme for a GCM. This notwithstanding, the scheme for calculating radiative heating in the UCLA multi-layered GMC is presented in this study. A brief presentation, for the UCLA two-layer GCM, has been given earlier by Arakawa, Katayama and Minz (1969).

II. LONG WAVE RADIATION

1. Basic equations

The atmospheric long wave (thermal) radiation with wavelengths between 2.5 μ and 40 μ is mainly affected by the absorption by water vapor, carbon dioxide and ozone. The scattering of long wave radiation by air molecules is negligible, but the scattering by large aerosol particles in the air and water droplets in a cloud layer may be significant. Because the present UCLA GCM covers only the troposphere, the absorption by ozone will be neglected. ~~Furthermore, for simplicity, any scattering of long wave radiation is assumed to be negligible.~~ However, for simplicity, the long wave scattering will be neglected.

By solving the equation of radiative transfer, subject to the boundary conditions that the downward long wave radiation flux is zero at the top of the atmosphere (troposphere), and the upward long wave radiation flux at the earth's surface is that given by black body radiation at the surface temperature, the downward and upward radiation fluxes $R^{\downarrow}_z$ and $R^{\uparrow}_z$ at a reference level z, can be expressed by:

$$R^{\downarrow}_z = \int_0^{\infty} \pi B_\nu(T_z)\, d\nu - \int_0^{\infty} \pi B_\nu(T_\infty)\, \tau_f \{k_\nu(u_\infty - u_z)\}\, d\nu$$

$$+ \int_0^{\infty} \int_{T_z}^{T_\infty} \pi \frac{dB_\nu(T)}{dT} \tau_f \{k_\nu(u - u_z)\}\, dT d\nu , \qquad (II.1)$$

$$R^{\uparrow}_z = \int_0^{\infty} \pi B_\nu(T_z)\, d\nu + \int_0^{\infty} \int_{T_z}^{T_s} \pi \frac{dB_\nu(T)}{dT} \tau_f \{k_\nu(u_z - u)\}\, dT d\nu , \qquad (II.2)$$

where $u(z)$ is the amount of absorbing medium (water vapor and carbon dioxide) in the vertical air column from the earth's surface to the level z, $T(z)$ is the temperature, $\pi B_\nu(T)$ is the flux of black body radiation of frequency ν at temperature T, k_ν is the generalized absorption coefficient defined by Elsasser (1942) and $\tau_f\{k_\nu u\}$ is the transmission

function of a slab at frequency ν. The subscripts g, z and ∞ denote the earth's surface, the reference level and the top of the atmosphere, respectively.

Since the width of an absorption line increases by collision damping, the absorption coefficient ℓ_ν is a function of pressure p. This effect can be approximately expressed by $(p/p_{oo})^a$ where p_{oo} is a standard pressure and a is a pressure scaling factor. Since the absorption coefficient is always multiplied by the amount of the absorbing medium u, we can conveniently use the absorption coefficient at the standard pressure and apply the pressure correction to u. The water vapor amount modified in this manner, the effective water vapor amount $u^*(z)$, is given by

$$u^* = \frac{1}{g}\int_{p(z)}^{p_g} q\left(\frac{p}{p_{oo}}\right)^a dp \qquad (II.3)$$

where q is the mixing ratio of water vapor. In the following discussion, u^* is used in lieu of u.

We define two types of weighted mean transmission function as follows:

$$\tau(u^*,T) = \tau(u^*_{H_2O}, u^*_{CO_2}, T) \qquad \tau(u^*,T) \equiv \frac{1}{\pi\frac{dB(T)}{dT}}\int_0^\infty \pi\frac{dB_\nu(T)}{dT}\tau_f(\ell_\nu u)\,d\nu \qquad (II.4)$$

$$\tilde{\tau}(u^*,T) = \tilde{\tau}(u^*_{H_2O}, u^*_{CO_2}, T) \qquad \tilde{\tau}(u^*,T) \equiv \frac{1}{\pi B(T)}\int_0^\infty \pi B_\nu(T)\,\tau_f(\ell_\nu u)\,d\nu \qquad (II.5)$$

where

$$\pi B(T) = \int_0^\infty \pi B_\nu(T)\,d\nu = \sigma T^4 \quad . \qquad (II.6)$$

Relation (II.6) is the Stefan-Boltzmann law and σ, the Stefan-Boltzmann constant, is 0.817×10^{-10} ly $min^{-1}\,{}^oK^{-4}$ (1.17×10^{-7} ly $day^{-1}\,{}^oK^{-4}$). τ and $\tilde{\tau}$ are functions of temperature because the spectrum distribution of black body radiation gradually changes with temperature. Yamamoto (1952) calculated the mean transmission function $\tau(u^*, T)$ for water vapor and found that: 1) the dependence of τ

on temperature is weak in the range 210°K to 320°K and 2) below 210°K, τ decreases very rapidly with decreasing temperature. Therefore, following Manabe and Möller (1961), if we select some critical temperature T_c near 220°K, $\tau(u^*, T)$ may be approximated for $T > T_c$ either by $\tau(u^*, \bar{T})$ with, say, $\bar{T} = 260°K$, say or by a mean transmission function averaged over the range 210°K to 320°K. Also, $\tilde{\tau}(u^*, T)$ may be approximated by $\tilde{\tau}(u^*, T_c)$.

The calculation procedure for long wave radiation is considerably simplified by use of the mean transmission functions. The second term of the right hand side of (II.1) is rewritten as follows:

$$\int_0^\infty \pi B_\nu(T_\infty)\, \tau_f\{\ell_\nu(u_\infty - u_z)\}\, d\nu$$

$$= \int_0^\infty \pi B_\nu(T_c)\, \tau_f\{\ell_\nu(u_\infty - u_z)\}\, d\nu + \int_0^\infty \int_{T_c}^{T_\infty} \pi \frac{dB_\nu}{dT}\, \tau_f\{\ell_\nu(u_\infty - u_z)\}\, dT d\nu ,$$

$$= \pi B(T_c)\, \tilde{\tau}(u_\infty^* - u_z^*, T_c) + \int_{T_c}^{T_\infty} \tau(u_\infty^* - u_z^*, \bar{T})\, \pi \frac{dB}{dT}\, dT ,$$

$$= \sigma T_c^4\, \tilde{\tau}(u_\infty^* - u_z^*, T_c) + (\sigma T_\infty^4 - \sigma T_c^4)\, \tau(u_\infty^* - u_z^*, \bar{T}) .$$

Substituting this relation into (II.1) we obtain

$$R_z^\downarrow = \pi B_z - \pi B_c\, \tilde{\tau}(u_\infty^* - u_z^*, T_c) - (\pi B_\infty - \pi B_c)\, \tau(u_\infty^* - u_z^*, \bar{T}) + \int_{\pi B_z}^{\pi B_\infty} \tau(u^* - u_z^*, \bar{T})\, d(\pi B) , \qquad (II.7)$$

where $\pi B_i \equiv \sigma T_i^4$.

Similarly, the upward flux at level z is

$$R^{\uparrow}_{z} = \pi B_{z} + \int_{\pi B_z}^{\pi B_g} \tau(u_z^* - u^*, \bar{T})\, d(\pi B) \,. \qquad (II.8)$$

The net upward flux at level z becomes

$$R_z \equiv R^{\uparrow}_{z} - R^{\downarrow}_{z} = A + B + C \,. \qquad (II.9)$$

where

$$A = \pi B_c\, \tilde{\tau}(u_\infty^* - u_z^*, T_c) \,,$$

$$B = (\pi B_\infty - \pi B_c)\, \tau(u_\infty^* - u_z^*, \bar{T}) \,,$$

$$C = \int_{\pi B_\infty}^{\pi B_z} \tau(u^* - u_z^*, \bar{T})\, d(\pi B) + \int_{\pi B_z}^{\pi B_g} \tau(u_z^* - u^*, \bar{T})\, d(\pi B) \,,$$

$$= \int_{-\pi B_\infty}^{\pi B_g} \tau(|u^* - u_z^*|, \bar{T})\, d(\pi B) \,. \qquad (II.10)$$

The relations above are schematically illustrated by Yamamoto's Radiation Chart shown in Figure II.1. → II-1.

The heating rate due to long wave radiation is given by

$$\frac{\partial \bar{T}}{\partial t} = \frac{g}{c_p} \frac{\partial R_z}{\partial p} \,, \qquad (II.11)$$

where g is the acceleration of gravity and c_p is the specific heat of air at constant pressure.

Turn figure around.
Reduce width of figure to fit the width of the page, with margins.

Top of page

Reduce size (on the Eng. Xerox machine, or photographically — Jim will know which to do)

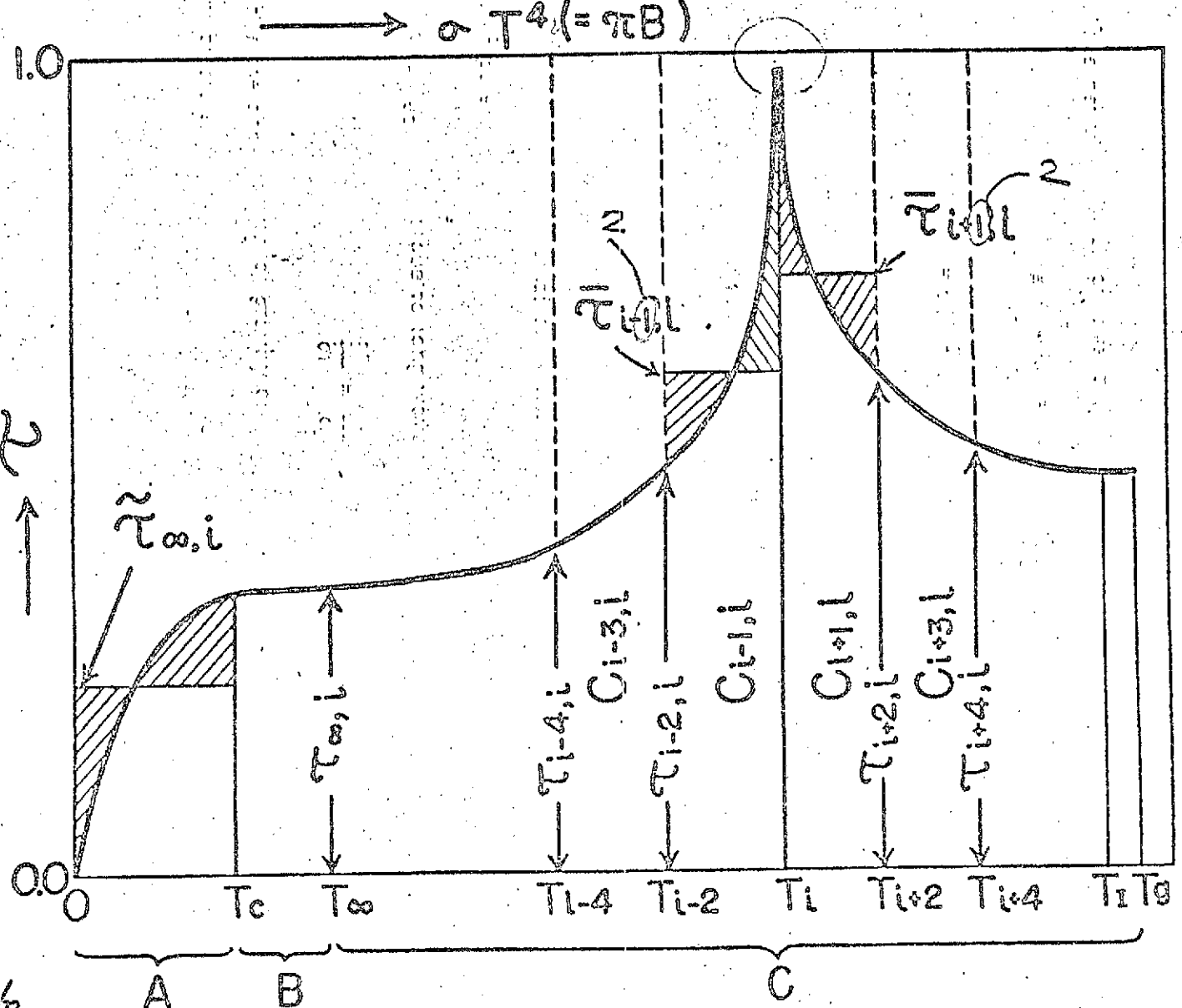

Figure 1

6

II-5

Add legend to [illegible] (1957) ← see p. iv.

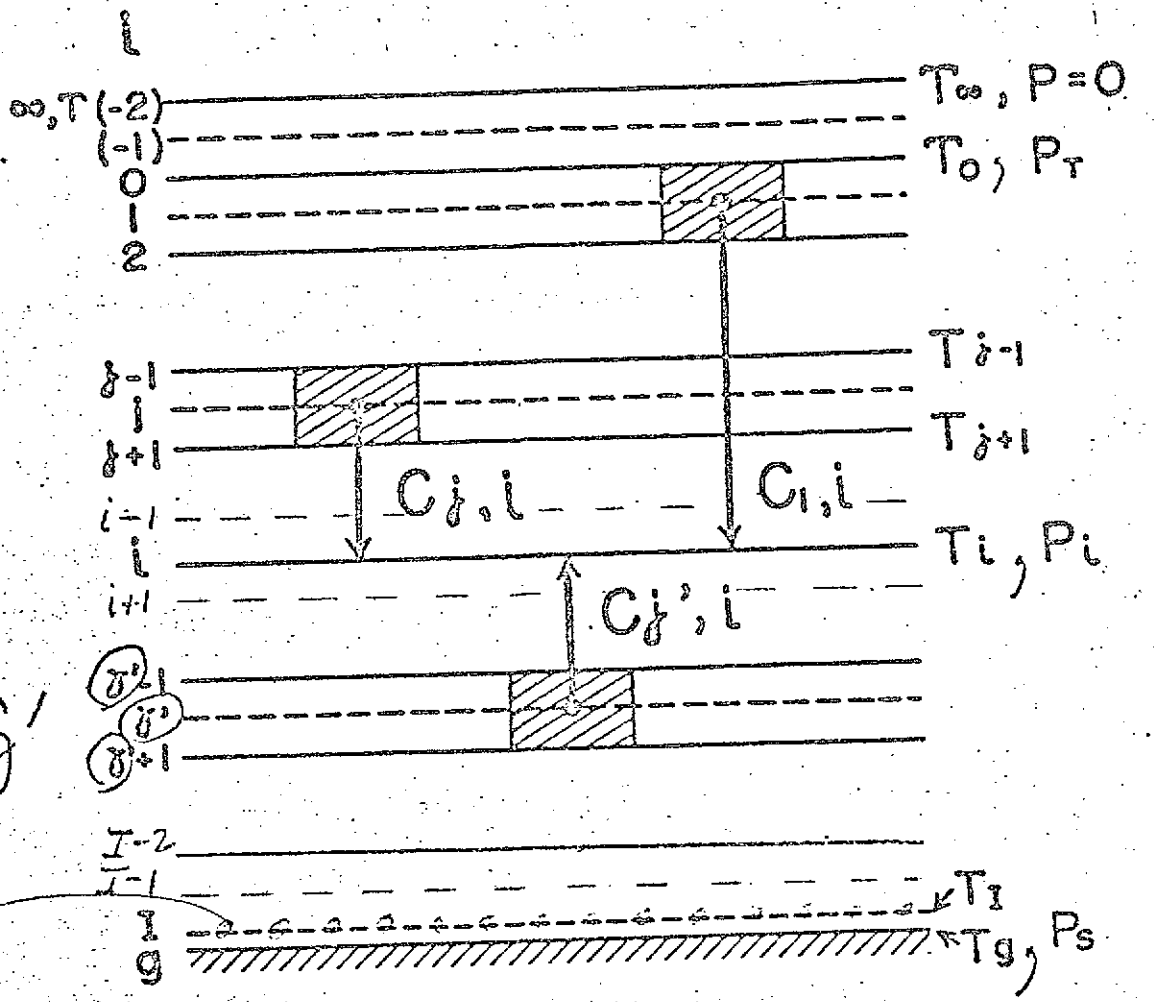

Should not be dashed

Fig. II-2. Indexing scheme for the levels of the model.

Figure 2

However, τ exponentially decreases as $|u^* - u_i^*|$ increases and the change of $|u^* - u_i^*|$ with πB is also roughly exponential. As shown in Figure II-1, τ in the neighborhood of level i usually decreases more rapidly with πB than a linear relationship. Therefore a careful formulation is required to compute the contribution to reference level i from its adjacent layers, $C_{i-1,i}$ and $C_{i+1,i}$.

To parameterize this contribution, a bulk transmission function $\bar{\tau}$ is defined as follows:

$$C_{i-1,i} = \int_{\pi B_{i-2}}^{\pi B_i} \tau(u^* - u_i^*, \bar{T})\, d(\pi B) \equiv (\pi B_i - \pi B_{i-2})\bar{\tau}_{i-2,i} \quad , \tag{II.16}$$

$$C_{i+1,i} = \int_{\pi B_i}^{\pi B_{i+2}} \tau(u_i^* - u^*, \bar{T})\, d(\pi B) \equiv (\pi B_{i+2} - \pi B_i)\bar{\tau}_{i+2,i} \quad . \tag{II.17}$$

Since $\tau = 1$ for $|u^* - u_i^*| = 0$, $\bar{\tau}_{i-2,i}$ (or $\bar{\tau}_{i+2,i}$) must have some value between 1 and $\tau_{i-2,i}$ (or $\tau_{i+2,i}$). Thus we define a linear interpolation factor m by the following relations:

$$\bar{\tau}_{i-2,i} = (1 + m_{i-2,i}\,\tau_{i-2,i})/(1+m_{i-2,i}) \quad , \tag{II.18}$$

$$\bar{\tau}_{i+2,i} = (1 + m_{i+2,i}\,\tau_{i+2,i})/(1+m_{i+2,i}) \quad . \tag{II.19}$$

The values of m must be determined by the physical parameters of the adjacent layer under consideration. We assume that the vertical distributions of the water vapor mixing ratio q and the temperature T can be represented by

$$q = q_i(p/p_i)^{k_i} \quad , \tag{II.20}$$

$$T = T_i + \Gamma_i(p_i - p) \quad . \tag{II.21}$$

Thus, m may be a function of pressure, mixing ratio and temperature at the reference level i, the lapse rate parameters k_i and Γ_i and the pressure thickness Δp of the layer (see Figure II-3). Thus,

$$m_i^{\pm} = f^{\pm}(p_i, q_i, T_i, k_i, \Gamma_i, \Delta p) \quad , \tag{II.22}$$

where $m_i^+ \equiv m_{i+2,i}$ and $m_i^- \equiv m_{i-2,i}$.

Retrieve by Inspect 3

For the GCM atmosphere, in which the above parameters may vary over a wider range than that observed in the real atmosphere, the integrals in (II.16) and (II.17) are computed numerically by dividing the GCM layer under consideration into thin sublayers of 10 mb thickness. In this way, the values

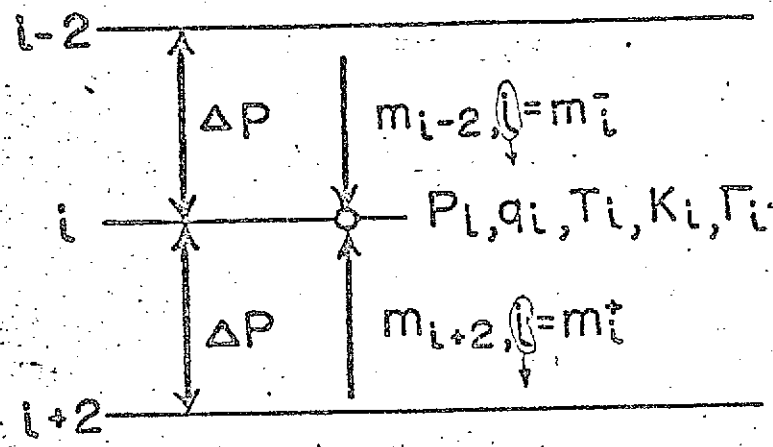

Fig. II-3. Schematic chart for the parameterization of the interpolation factor. ~~Figure 3~~ m.

of $\bar{\tau}_i^{\pm}$ were estimated from (II.16) and (II.17). Then, from (II.18) and (II.19), the values of $m_i^{\pm}$ here were obtained as a function of p_i, q_i, T_i, k_i, Γ_i and Δp. The functional form of $m_i^{\pm}$ was then found by a curve fitting technique.

These preliminary calculations have shown that the dependence of $m_i^{\pm}$ on T_i is negligibly small; it is therefore ignored. Figure II-4 shows that $m_i^{\pm}$ can be expressed approximately as a linear function of Δp when the values of the remaining parameters are fixed. Thus,

$$m_i^{\pm} = a_i^{\pm} + b_i^{\pm}\,\Delta p/100 \,, \qquad \text{(II.23)}$$

where $a_i^{\pm}$ and $b_i^{\pm}$ may be functions of p_i, q_i, k_i and Γ_i. Since the dependence of $a_i^{\pm}$ on k_i and Γ_i is weak, it is neglected and the following empirical relations are obtained:

Fig 11-4. Interpolation factor . . . . . , respectively.

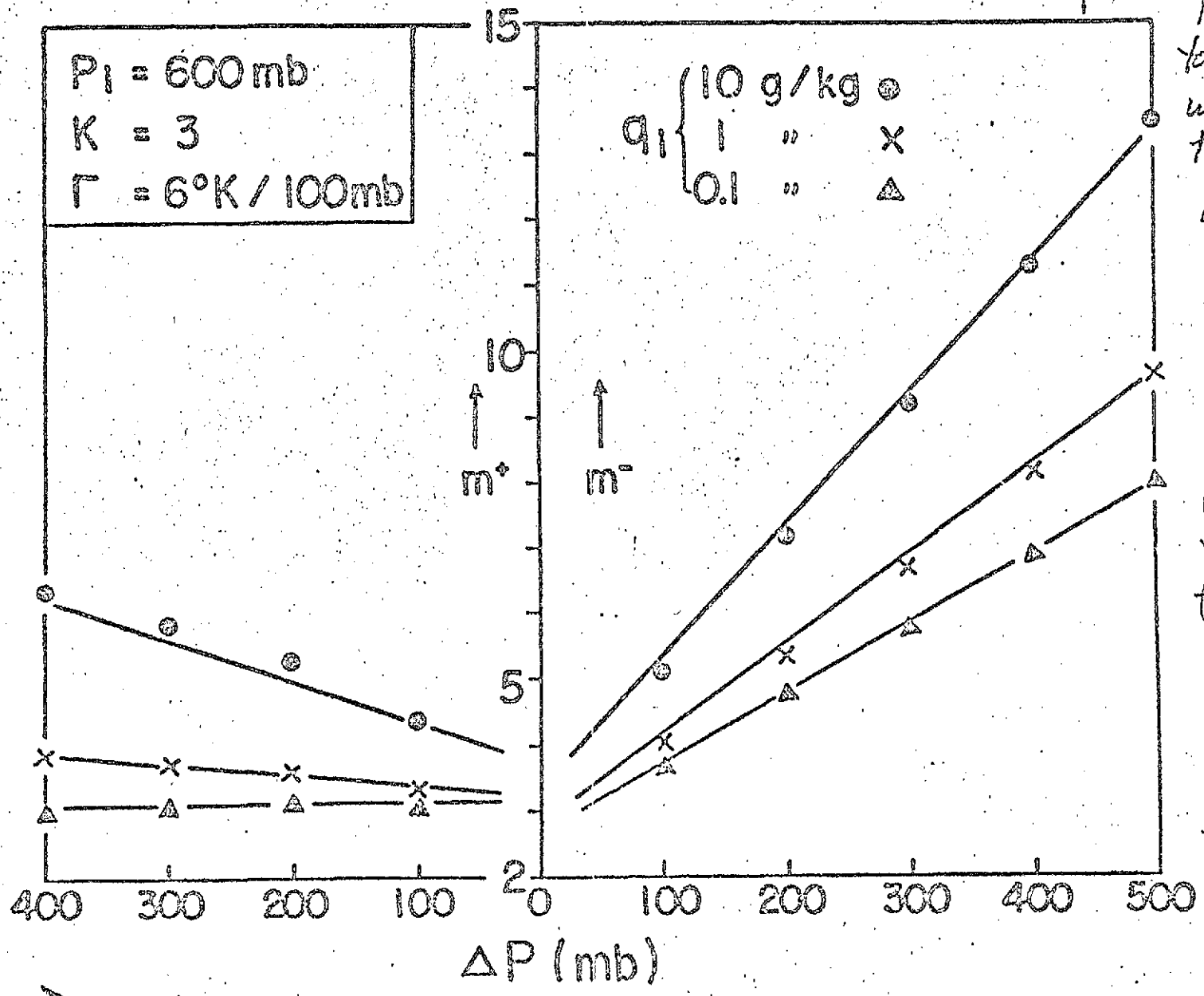

Top of page

Reduce figure to fit the width of the page, when turned around, with margins

11-10

(You can reduce the figure size on the Engineering Xerox machine)

$$a_i^+ = L_a^+(P_i) + F_a^+(Z_i) , \tag{II.24}$$

$$b_i^+ = L_b^+(P_i) + F_b^+(Z_i) + \left(\frac{\partial b}{\partial k}\right)^+ \Delta k_i + \left(\frac{\partial b}{\partial \Gamma}\right)^+ \Delta \Gamma_i . \tag{II.25}$$

$$L_a^+(P_i) = -1.66 + 1.76 \log_{10} P_i ,$$

$$L_b^+(P_i) = -0.197 + 0.0002 P_i ,$$

$$F_a^+(Z_i) = 0.30 Z_i + 0.28 Z_i^{②} + 0.04 Z_i^{③} ,$$

$$F_b^+(Z_i) = 0.0812 Z_i - 0.045 Z_i^{②} + 0.02334 Z_i^{③} ,$$

$$\left(\frac{\partial b}{\partial \Gamma}\right)^+ = \text{Min}\,(-0.041 + 0.021 Z_i, -0.06) < 0 ,$$

$$\left(\frac{\partial b}{\partial \Gamma}\right)^+ = \text{Max}\,(0.01225 + 0.007 Z_i, 0.0093) > 0 .$$

$$a_i^- = -0.09 L_a^-(P_i) + F_a^-(Z_i - 0.105 L_a^-(P_i)) , \tag{II-26}$$

$$b_i^- = -0.09 L_b^-(P_i) + F_b^-(Z_i - 0.105 L_b^-(P_i)) + \left(\frac{\partial b}{\partial k}\right)^- \Delta k_i + \left(\frac{\partial b}{\partial \Gamma}\right)^- \Delta \Gamma_i . \tag{II.27}$$

$$L_a^-(P_i) = \text{Max}\,(61.86 - 22.92 \log_{10} P_i, 76.63 - 28.39 \log_{10} P_i) ,$$

$$L_b^-(P_i) = \text{Min}\,(-42.59 + 15.78 \log_{10} P_i, -60.81 + 22.53 \log_{10} P_i) ,$$

$$F_a^-(X) = 2.57 + 0.233 X + 0.18 X^{②} + 0.027 X^{③} ,$$

$$F_b^-(X) = 1.42 + 0.48 X + 0.16 X^{②} + 0.011 X^{③} ,$$

$$\left(\frac{\partial b}{\partial k}\right)^- = 0.08 + (0.371 - 0.102 \log_{10} P_i)(Z_i + 2.1) > 0 ,$$

$$\left(\frac{\partial b}{\partial \Gamma}\right)^- = \text{Min}\,(-0.0325 - 0.005 Z_i, -0.0275) < 0 ,$$

where $Z_i = \log_{10} q_i$, $Z_1 = |Z_i + 2.5|$, $\Delta k_i = k_i - 3$, $\Delta\Gamma_i = \Gamma_i - 10$ (°K/100 mb) and X is a dummy variable.

Figure II-4 shows the relation between $m_i^{\pm}$ and Δp for the cases of q_i = 10, 1, 0.1 g/Kg, p_i = 600 mb, k_i = 3 and Γ_i = 6°K/100 mb. The plotted points give the values of $m_i^{\pm}$ obtained from equations (II.16) - (II.19), while the straight lines represent $m_i^{\pm}$ determined from (II.23) - (II.27). The agreement is satisfactory.

The values of $a_i^{\pm}$ and $b_i^{\pm}$ for various values of p_i and q_i are presented in Table II-1 for the case of k_i = 3, Γ_i = 6°K/100 mb. $a_i^{\pm}$ and $b_i^{\pm}$ increase while b_i^- decreases as p_i increases. Their dependence on q_i is not monotonic. $a_i^{\pm}$ gradually decrease with decreasing mixing ratio and reach minimum values near q_i = 0.1 g/Kg. $b_i^{\pm}$ exhibit a similar behavior with minimum values near q_i = 0.01 g/Kg. Since b_i^+ is considerably smaller than b_i^-, while the difference between a_i^+ and a_i^- is usually less than 1, m_i^- is larger than m_i^+ in most cases.

As discussed in Appendix C, if the permissible error in the heating rate $C_{i-1,i}$ and $C_{i+1,i}$ is 0.2 °C/day, the accuracy requirement for $m_i^{\pm}$ is not too severe and usually more than 20% error in $m_i^{\pm}$ can be tolerated.

If the vertical coordinate of a GCM is pressure or geopotential height, p_i and Δp are exactly or nearly constant in space and time. For such a GCM, only q_i, k_i and Γ_i are variable parameters in the expression for $m_i^{\pm}$. Considering the range of these parameters in the actual atmosphere, appropriate mean values for k_i and Γ_i, such as their globally averaged climatological values, may be used in the empirical expressions for $m_i^{\pm}$. For example, $k \simeq 3$ and $\Gamma \simeq 6$°K/100 mb may be adopted.

TABLE II-1. The values of $a_i^{\pm}$ and $b_i^{\pm}$ for various p_i and q_i. The values of $b_i^{\pm}$ are shown for the case of $k_i = 3$, $\Gamma_i = 6°K/100$ mb.

	P_i(mb)	q_i(g/Kg)					
		30	10	1	0.1	0.01	0.001
a_i^+	100	3.05	2.48	1.86	1.80	2.06	2.40
	200	3.58	3.01	2.39	2.33	2.59	2.94
	400	4.11	3.54	2.92	2.86	3.12	3.46
	600	4.42	3.85	3.23	3.17	3.43	3.77
	800	4.64	4.07	3.45	3.39	3.65	3.99
	1000	4.81	4.24	3.62	3.56	3.82	4.16
b_i^+	100	0.81	0.48	0.06	-0.12	-0.18	-0.18
	200	0.83	0.50	0.08	-0.10	-0.16	-0.16
	400	0.87	0.54	0.12	-0.06	-0.12	-0.12
	600	0.91	0.58	0.16	-0.02	-0.08	-0.08
	800	0.95	0.62	0.20	0.03	-0.04	-0.04
	1000	0.99	0.66	0.24	0.07	-0.00	-0.00
a_i^-	200	1.64	1.52	1.49	1.62	1.77	1.75
	400	2.90	2.59	2.27	2.26	2.41	2.54
	600	3.75	3.31	2.79	2.65	2.74	2.90
	800	4.36	3.83	3.15	2.92	2.96	3.11
	1000	4.87	4.27	3.47	3.14	3.13	3.28
b_i^-	200	4.64	3.99	2.96	2.31	2.00	1.93
	400	3.12	2.62	1.87	1.45	1.32	1.39
	600	2.43	2.00	1.38	1.06	1.02	1.15
	800	2.06	1.67	1.12	0.86	0.85	1.01
	1000	1.79	1.43	0.92	0.71	0.73	0.91

As a rough approximation, the effect of the variation of q_i may also be ignored. In that case, the hemispheric mean climatological value given by (IV.16) is recommended as an appropriate constant value of q. However, the mixing ratio at a reference level in the lower troposphere varies by more than two orders of magnitude over the global domain. Therefore, it is desirable to retain the spatial and temporal variation of q for the estimation of $m_i^{\pm}$.

When the σ-coordinate system is employed, as in the UCLA GCM, p_i on a σ-level and Δp between σ-levels may vary in space and time. For example, over high mountain areas such as the Himalayas and the Antarctic continent, p_i and Δp are significantly reduced, which leads to a decrease in $m_i^{\pm}$ and an increase in $\bar{\tau}_i^{\pm}$. If p_i is assumed constant on a reference σ-level, the contribution to the flux of long wave radiation at the reference level from its adjacent layers is underestimated over high mountain areas.

Change section 3 to section 4 and move accordingly

3. The effect of clouds

When the sky is covered by a thick cloud, the top and bottom of the cloud may be treated as perfect black body radiators at their respective temperatures (the net flux in the cloud is assumed to be zero). This assumption can safely be made for a dense cloud, but it must be checked for cirriform clouds which contain small amounts of water vapor and solid water (ice crystal concentrations less than $0.1\ (g\,m^{-3})$.

Fritz and Winston (1962) analyzed the radiation measurements of TIROS II and found that the cirrostratus layer did not strongly absorb in the window region of long wave radiation, 8 μ - 12 μ. A detailed discussion of the greyness of cirriform clouds has been presented by Katayama (1966). Because

Cirriform clouds do not completely absorb long wave radiation, we assume, for simplicity, that they behave as grey body radiators with greyness of 0.5. In the computation of the radiation flux, the above assumption is introduced roughly by modifying the amount of cirriform clouds by the weighting factor of 0.5.

It has been confirmed by laboratory experiments that there is a critical temperature, about -40°C, at which homogeneous nucleation transforms all liquid water to ice crystals. Clodman (1957) found from aircraft observations that the base of cirrus clouds is situated at the level where the air temperature is about -40°C. We therefore assume that any non-convective cloud formed in a layer with temperature less than -40°C is cirriform and that the greyness of the cloud is 0.5

Change section 4 to section 3 and move accordingly

(4) Empirical transmission function equations

According to Yamamoto (1952), the total transmission function of a mixture of water vapor and carbon dioxide is assumed to be represented by the product of their respective transmission functions, that is

$$\tau(u^*_{H_2O}, u^*_{CO_2}, T) = \tau_{H_2O}(u^*_{H_2O}, T)\, \tau_{CO_2}(u^*_{CO_2}, T) \quad . \qquad (II.28)$$

Using the table presented by Yamamoto (1952), we deduce the following empirical equations for the transmission functions of water vapor and carbon dioxide.

(i) Water vapor

Two empirical equations for the transmission function of water vapor at a temperature of 260°K are presented below; the first has a form similar to Callendar's expression (1941) for carbon dioxide while the second is expressed

by a quadratic polynomial

$$(A)\quad \tau_{H_2O}(u^*, 260^\circ K) = \frac{1}{1+1.750\, u^{*0.416}}\ , \qquad (II.29)$$

$$(B)\quad \tau_{H_2O}(u^*, 260^\circ K) = 0.384 - 0.2785\, Z + 0.0345\, Z^2,\ (u^* \geq 1)\ ,$$

$$= 0.384 - 0.259\, Z - 0.028\, Z^2,\ (10^{-4} \leq u^* < 1), \qquad (II.30)$$

$$= 1/(1+288\, u^*),\ (u^* < 10^{-4})\ ,$$

where $Z = \log_{10} u^*$ and $u^* = u^*_{H_2O}$.

Table II-2 shows the accuracy of the two expressions above. In the real atmosphere, u^* is usually less than 6 g cm^{-2}. Therefore the maximum error of expression A is about 0.025 while expression B has a negligibly small error for u^* between 10 g cm^{-2} and 0.0001 g cm^{-2}.

TABLE ~~II-2.~~ II-2. Accuracy of the empirical equations for the transmission function of water vapor at a temperature of 260°K. The errors are shown in units of 10^{-3}.

$u^*_{H_2O}$ (g cm^{-2})	$\tau_{H_2O}(u^*_{H_2O}, 260^\circ K)$				
	Obs.	A	O-A	B	O-B
10	0.140	0.180	-40	0.140	0
6	0.188	0.212	-24	0.188	0
3	0.259	0.266	- 7	0.259	0
1	0.384	0.364	20	0.384	0
0.3	0.510	0.485	25	0.512	-2
0.1	0.612	0.598	14	0.615	-3
0.03	0.713	0.711	2	0.714	-1
0.01	0.790	0.795	- 5	0.790	0
0.001	0.910	0.910	0	0.909	1
0.0001	0.972	0.963	9	0.972	0

TABLE ~~II-3.~~ 11-3. Accuracy of the empirical equations for the transmission function of water vapor averaged over the temperature range between 220° and 300°K. The errors are shown in units of 10^{-3}.

$u^*_{H_2O}$	$\tau^A_{H_2O}(u^*_{H_2O})$						
($g\ cm^{-2}$)	Obs.	C	O-C	D	O-D	E	O-E
10	0.134	0.172	-28	0.134	0	0.134	0
6	0.181	0.204	-23	0.185	-4	0.181	0
3	0.250	0.268	-18	0.248	2	0.250	0
1	0.373	0.364	-9	0.373	0	0.373	0
0.3	0.499	0.489	10	0.498	1	0.501	-2
0.1	0.603	0.597	6	0.601	2	0.605	-2
0.03	0.704	0.715	-11	0.704	0	0.705	-1
0.01	0.783	0.800	-17	0.784	-1	0.782	1
0.001	0.905	0.914	-9	0.905	0	0.904	1
0.0001	0.971	0.966	5	0.969	2	0.971	0

As previously mentioned, the transmission function of a slab of water vapor is nearly constant with respect to temperature; it varies by about 0.02 from 220°K to 300°K. It may therefore be more suitable to use an averaged value of the transmission function over this temperature range rather than the value at 260°K. We define $\tau^A_{H_2O}$ as

$$\tau^A_{H_2O}(u^*) = \tfrac{1}{3}[\tau_{H_2O}(u^*, 300^\circ K) + \tau_{H_2O}(u^*, 260^\circ K) + \tau_{H_2O}(u^*, 220^\circ K)] \quad (11.31)$$

The observed values of $\tau^A_{H_2O}$ are shown in the second column of Table II-3. From the observed values, three different empirical expressions are deduced as follows:

$$(C)\quad \tau^{A}_{H_2O}(u^*) = \frac{1}{1+1.746\,u^{*0.423}} \qquad (II.32)$$

$$(D)\quad \tau^{A}_{H_2O}(u^*) = F(1.681,\ 0.535),\quad (u^* \geq 0.724)$$
$$= F(1.600,\ 0.3815),\quad (0.00186 \leq u^* < 0.724) \qquad (II.33)$$
$$= F(3.853,\ 0.522),\quad (u^* < 0.00186)$$

where $F(a,b) = 1/(1+au^{*b})$.

$$(E)\quad \tau^{A}_{H_2O}(u^*) = 0.373 - 0.274\,Z + 0.035\,Z^2,\quad (u^* \geq 1)$$
$$= 0.373 - 0.2595\,Z - 0.0275\,Z^2,\quad (10^{-4} \leq u^* < 1) \qquad (II.34)$$
$$= 1/(1+298.7\,u^*),\quad (u^* < 10^{-4})$$

Expressions (C) and (E) are similar to (A) and (B), respectively; expression (D) is an extension of (C). The accuracy of these three expressions is shown in Table II-3. Expression (C) exhibits the largest error, but its maximum error is less than 0.025 for $u^* \leq 6$ g cm^{-2}.

It is also necessary to evaluate $\tilde{\tau}(u^*, T)$, the mean transmission function defined by (II.5). As suggested in section II.1, 220°K is adopted as the critical temperature T_c. The empirical expressions for $\tilde{\tau}$ are similar to those for τ, namely

$$(A')\quad \tilde{\tau}_{H_2O}(u^*, 220^\circ K) = \frac{1}{1+3.0\,u^{*0.408}} \qquad (II.35)$$

$$(B')\quad \tilde{\tau}_{H_2O}(u^*, 220^\circ K) = 0.254 - 0.1985\,Z + 0.0205\,Z^2,\quad (0.1 \leq u^* < 10)$$
$$= 0.216 - 0.2827\,Z - 0.0258\,Z^2,\quad (10^{-4} \leq u^* < 0.1)$$

The observed values of $\tilde{\tau}$ are shown in the second column of Table (II.36)

From the observed values

$$= 1/(1+2.56\,u^{*0.39}),\quad (u^* < 10^{-4})$$

are fitted

$$(C')\quad \tilde{\tau}_{H_2O}(u^*, 220^\circ K) = 0.254 - 0.2224\,Z + 0.0444\,Z^2,\quad (1 \leq u^* < 10)$$
$$= 0.254 - 0.226\,Z - 0.007\,Z^2,\quad (0.03 \leq u^* < 1) \qquad (II.37)$$
$$= 0.194 - 0.297\,Z - 0.028\,Z^2,\quad (10^{-4} \leq u^* < 0.03)$$

The accuracy of these empirical expressions is shown in Table II-4.

Expressions (A) and (A') were used for τ_{H_2O} and $\tilde{\tau}_{H_2O}$, respectively, in the 2-layer moist and early-stage 3-layer UCLA general circulation models. In the current 3-layer UCLA GCM, expressions (E) and (B') have been adopted for τ_{H_2O} and $\tilde{\tau}_{H_2O}$, respectively.

TABLE II-4. Accuracy of the empirical equations for $\tilde{\tau}_{H_2O}$ at the temperature of 220°K. The errors are shown in unit of 10^{-3}.

$u^*_{H_2O}$	$\tilde{\tau}_{H_2O}(u^*_{H_2O}, 220°K)$						
(g cm^{-2})	Obs.	A'	O-A'	C'	O-C'	B'	O-B'
10	0.076	0.115	-39	0.076	0	0.076	0
3	0.158	0.176	-18	0.158	0	0.164	-6
1	0.254	0.250	4	0.254	0	0.254	0
0.3	0.368	0.353	15	0.370	-2	0.366	2
0.1	0.473	0.460	13	0.473	0	0.473	0
0.03	0.584	0.582	2	0.582	2	0.585	-1
0.01	0.676	0.685	-9	0.676	0	0.678	-2
0.001	0.833	0.848	-15	0.833	0	0.832	1
0.0001	0.934	0.935	1	0.934	0	0.934	0
0.00001	0.972	0.973	1	0.979	-7	0.985	-13

(ii) Carbon dioxide

The transmission function of carbon dioxide at normal temperature and pressure (NTP) is shown in Table II-5. These observations can be expressed by

$$\tau_{CO_2}(u^*_{CO_2}) = 0.930 - 0.066 \log_{10} u^*_{CO_2}, \quad \text{for } u^*_{CO_2} \geq 0.3 \text{ cm - NTP} \qquad (11.38)$$

where $u^*_{CO_2}$ is the effective amount of carbon dioxide at NTP within a layer of thickness $|p_i - p_j|$ (see section IV.2, equation (IV.19)). The agreement between (II.38) and the observations is good, as shown in Table II-5. Introducing (IV.19) into (II.38) yields

$$\tau_{CO_2}(i,j) = 0.791 - 0.066 \log_{10}\left[\frac{|p_i^2 - p_j^2|}{p_\infty^2}\right] . \qquad (II.39)$$

The temperature dependence of the transmission function of carbon dioxide is neglected in the present formulation.

TABLE II-5. The transmission function of carbon dioxide. Calc. shows the value obtained from equation (II.38).

$u^*_{CO_2}$ (cm/NTP)		1	3	10	30	100	150
τ_{CO_2}	Obs.	0.930	0.900	0.865	0.834	0.796	0.784
	Calc.	0.930	0.899	0.864	0.833	0.798	0.786

If pressure is the vertical coordinate of a GCM, $\tau_{CO_2}(i,j)$ does not change in space or time. In the σ-coordinate system, however, because the pressure at a constant σ-level varies with the surface pressure, p_s, $\tau_{CO_2}(i,j)$ also varies with p_s. Thus, with the exception of the layer above the $\sigma \cong 0$ level, $\tau_{CO_2}(i,j)$ must be calculated at each grid point and each time step. From an examination of the dependence of $\tau_{CO_2}(i,j)$ on p_s, the following simplified empirical relation is adopted:

$$\tau_{CO_2}(i,j;p_s) = \beta\, \tau_{CO_2}(i,j;p_\infty) , \qquad (II.40)$$

where

$$\beta = 1 + 0.09(1 - p_s/p_\infty) , \qquad (II.41)$$

and $\tau_{CO_2}(i,j;p_s)$ is $\tau_{CO_2}(i,j)$ when the surface pressure is p_s and $p_{oo} = 1000$ mb. Figure II-5 shows the values of $\tau_{CO_2}(i,j;p_{oo})$ for various layers of the 3-layer GCM.

Finally, the total transmission function for the layer between levels i and j is given by

$$\tau_{ij} \equiv \tau(u^*_{H_2O}(i,j),\ u^*_{CO_2}(i,j),\ T)$$

$$= \beta(p_s)\,\tau_{CO_2}(i,j;p_{oo})\,\tau_{H_2O}(i,j) \qquad \text{(II.42)}$$

where $\tau_{H_2O}(i,j) = \tau_{H_2O}(|u^*_i - u^*_j|, \bar{T})$.

5. Finite difference schemes

In this section, the finite difference scheme for the long wave radiation calculation is summarized. The indexing scheme is shown in Fig. II-2. The following assumptions are made regarding cloud layers:

(i) a cloud layer is located about a level with an odd index

(ii) the cloud thickness is equal to the thickness of the layer in which it is situated

(iii) the distribution of cloud elements is horizontally quasi-homogeneous

(iv) there are no clouds in the layer above level 0

(v) the cloudiness and greyness of a cloud in layer j (between levels j-1 and j+1) are CL_j and α'_j, respectively; the modified cloudiness CL'_j is defined by $CL'_j = \alpha'_j\, CL_j$.

Combining (II.9) and (II.13), the net flux of long wave radiation at reference level i in a clear sky is

$$R_i = \pi B_c \tilde{\tau}_{\infty i} + (\pi B_\infty - \pi B_c)\,\tau_{\infty i} + \sum_{j=-1}^{I-1} C_{j,i} + (\pi B_g - \pi B_I)\,\tau_{Ii} \qquad \text{(II.43)}$$

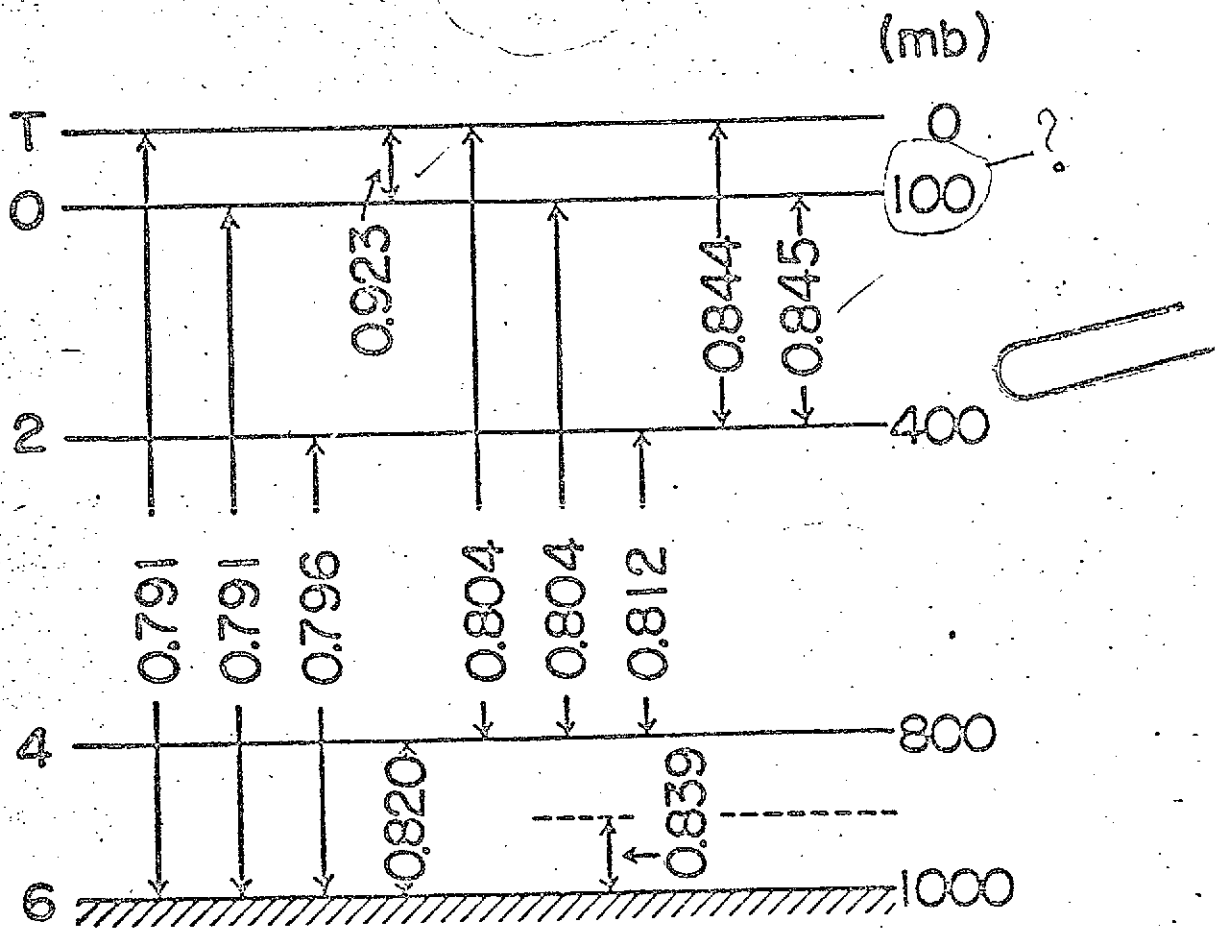

Fig. II-5. Transmission function of carbon dioxide for various layers.

~~Figure 5~~

In a cloudy sky, (II.43) is modified as

$$R_i = [\pi B_c \tilde{\tau}_{\infty i} + (\pi B_\infty - \pi B_c)\tau_{\infty i} + C_{-1,i} + C_{1,i}] \prod_{j=1}^{i-1}{}' (1-CL_j') + C_{3,i} \prod_{j=3}^{i-1}{}' (1-CL_j') + \cdots$$
$$+ C_{i-3,i}(1-CL_{i-3}')(1-CL_{i-1}') + C_{i-1,i}(1-CL_{i-1}')$$
$$+ C_{i+1,i}(1-CL_{i+1}') + C_{i+3,i}(1-CL_{i+1}')(1-CL_{i+3}')$$
$$+ \cdots + C_{I-3,i} \prod_{j=i+1}^{I-3}{}' (1-CL_j')$$
$$+ [C_{I-1,i} + (\pi B_g - \pi B_I)\tau_{Ii}] \prod_{j=i+1}^{I-1}{}' (1-CL_j') \qquad (II.44)$$

where $\prod_j'$ denotes multiplication over j odd. τ_{ij} is expressed by (II.42).

Substituting (II.14) and (II.16) - (II.19) into the above relation yields

$$R_i = \Big(\sigma T_c^4 \tilde{\tau}_{\infty i} + \Delta B_{c,\infty}\tau_{\infty i} + \Delta B_{\infty,o}\frac{\tau_{\infty i}+\tau_{oi}}{2}$$
$$+ \Delta B_{o,2}\frac{\tau_{oi}+\tau_{2i}}{2}\Big) \prod_{j=1}^{i-1}{}' (1-CL_j')$$
$$+ \Delta B_{2,4}\frac{\tau_{2i}+\tau_{4i}}{2} \prod_{j=3}^{i-1}{}' (1-CL_j') + \cdots$$
$$+ \Delta B_{i-4,i-2}\frac{\tau_{i-4,i}+\tau_{i-2,i}}{2}(1-CL_{i-3}')(1-CL_{i-1}')$$
$$+ \Delta B_{i-2,i}\frac{1+\bar{m}_i\tau_{i-2,i}}{1+\bar{m}_i}(1-CL_{i-1}')$$
$$+ \Delta B_{i,i+2}\frac{1+\bar{m}_i^{+}\tau_{i+2,i}}{1+\bar{m}_i^{+}}(1-CL_{i+1}')$$
$$+ \Delta B_{i+2,i+4}\frac{\tau_{i+2,i}+\tau_{i+4,i}}{2}(1-CL_{i+3}')(1-CL_{i+1}')$$
$$+ \cdots$$

$$+ \Delta B_{I-4,I-2} \frac{\tau_{I-4,i} + \tau_{I-2,i}}{2} \prod_{i=i+1}^{I-3} (1-CL_i^!)$$

$$+ \left(\Delta B_{I-2,I} \frac{\tau_{I-2,i} + \tau_{I,i}}{2} + \Delta B_{I,g} \tau_{I,i} \right) \prod_{i=i+1}^{I-1} (1-CL_i^!) \quad , \qquad (II.45)$$

where $\Delta B_{\ell,m} = \sigma T_m^4 - \sigma T_\ell^4$.

As an example, the finite difference scheme for the current UCLA 3-layer GCM is shown in Appendix A.

III. SOLAR RADIATION

There are three principal factors that contribute to the depletion of solar radiation in the cloudless troposphere:

(i) absorption by water vapor

(ii) Rayleigh scattering by air molecules

(iii) absorption and Mie scattering by aerosol particles

According to Katayama's preliminary result (1966), absorption by aerosol particles is comparable to absorption by a cloud layer in the normal mean cloud state and is of the same order as the absorption by water vapor in high latitudes at large sun zenith angles. Thus the depletion by aerosol absorption should be included in the atmospheric radiation process. At present, however, we do not know very much about the optical properties of aerosol particles nor about the spatial and temporal variation of the aerosol distribution, and, therefore, we are neglecting the absorption and Mie scattering of solar radiation by aerosol particles.

1. Basic quantities

The effective absorption bands of water vapor for the solar spectrum are in the wavelength range $\lambda > 0.9\,\mu$. There are two absorption bands in the region $\lambda < 0.9\,\mu$, namely $\lambda = 0.75\,\mu$ and $0.85\,\mu$, however their contribution to the total water vapor absorption is negligibly small.

On the other hand, since the amount of Rayleigh scattering is inversely proportional to the fourth power of the wavelength λ, the scattering by air molecules rapidly decreases with increasing wavelength. With an error of a few per cent, scattering in the wavelength range $\lambda > 0.9\,\mu$ can be neglected.

Based upon these considerations, Joseph (1966, 1970) divided the solar radiation into two components: the scattered and the absorbed parts. This idea

was also presented by Feigel'son (1964), using a critical wavelength of 0.75 μ instead of 0.9 μ. Thus, for $\lambda < 0.9\,\mu$, solar radiation is assumed to be Rayleigh scattered but not absorbed by water vapor, while for $\lambda > 0.9\,\mu$, the converse is assumed. The solar radiation incident at the top of the atmosphere is then separated as follows:

The scattered part: $$S_o^s = 0.651\, S_o \cos\zeta \qquad \text{(III.1)}$$

The absorbed part: $$S_o^a = 0.349\, S_o \cos\zeta \qquad \text{(III.2)}$$

where S_o is the solar constant and ζ is the zenith angle of the sun.

(i) Absorptivity of water vapor

Mügge and Möller (1932) found the following empirical relation for the absorption by water vapor of the mean solar constant:

$$a = 0.172\,(w^* \sec\zeta)^{0.303} \text{ ly min}^{-1},$$

where w^* is the effective water vapor amount.

Yamamoto and Onishi (1948) and MacDonald (1960) also constructed absorption curves. Their values are smaller than those of Mügge and Möller by about 15 per cent. Manabe and Möller (1961) recalculated the absorption and obtained a 10 per cent larger value than Mügge and Möller.

Since absorption by aerosol particles is neglected in the present treatment, Manabe and Möller's larger value of the absorption by water vapor,

$$a' \equiv 0.189\,(w^* \sec\zeta)^{0.303} \text{ ly min}^{-1}, \qquad \text{(III.3)}$$

is employed. Since this absorption refers to the mean solar constant $\bar{S}_o$, the absorptivity for the absorbed part is

$$\frac{a'}{0.349\bar{S}_o} = 0.271\,(w^* \sec\zeta)^{0.303}, \qquad \text{(III.4)}$$

where $\bar{S}_o = 2$ ly min^{-1}.

Defining the absorptivity function A(x) by

$$A(x) = 0.271\ (x)^{0.303}\ , \qquad \text{(III.5)}$$

the absorption by water vapor of the direct solar radiation is

$$a' = S_o^a\, A(u^* \sec\zeta)\ ,$$

$$= 0.349\, S_o \cos\zeta\, A(u^* \sec\zeta)\ , \qquad \text{(III.6)}$$

where $S_o = \bar{S}_o \left(\frac{\bar{r}_E}{r_E}\right)^2$, (Carter) (III.7)

and r_E is the sun's distance from the earth and $\bar{r}_E$ is the mean value of r_E, that is one astronomical unit. The zenith angle ζ is given by

$$\cos\zeta = \sin\varphi\ \sin\delta + \cos\varphi\ \cos\delta\ \cos h\ , \qquad \text{(III.8)}$$

where φ is the latitude, δ is the solar declination and h is the hour angle of the sun.

In a numerical simulation of the seasonal variation of the general circulation, the seasonal variation of δ and r_E must be ~~predicted or tabulated.~~ known. As shown in Appendix D, δ and r_E can be estimated by a perturbation solution of Kepler's second law.

(ii) The albedo of the cloudless atmosphere

The albedo of the ~~clear sky~~ cloudless atmosphere due to Rayleigh scattering was estimated by Coulson (1959) and is presented in Table II-3 of the paper by Joseph (1966). Joseph ~~tried to express~~ fitted the albedo by a least-squares polynomial in $\cos\zeta$, of the form

$$a_o(\zeta) = \sum_i C_i \cos^i\zeta\ .$$

In the following, the empirical expression

$$a_o(\zeta, p_s) = 0.085 - 0.245 \log_{10}\left(\frac{p_s}{p_{oo}}\cos\zeta\right) \qquad \text{(III.9)}$$

will be employed, where p_{oo} is 1000 mb and p_s is the surface pressure. Table III-1 gives a comparison of (III.9), for $p_s = p_{oo}$, with the values of Coulson. The error of (III.9) is less than 10 per cent.

TABLE III-1. The albedo of the cloudless atmosphere.

ζ		0°	36.9°	56.4°	78.5°	84.3°	88.8°
α_o	Coulson	.085	.097	.158	.234	.333	.519
	(III.9)	.085	.108	.148	.257	.331	.470

(iii) The albedo and absorptivity of clouds

The albedo and absorptivity of a cloud are functions of the cloud thickness, cloud height, liquid and/or solid water content, water vapor content and zenith angle of the sun. Since observations are sparse and theoretical studies are insufficient, it is not possible to introduce the above effects explicitly into the model. Therefore, following Rodgers (1967), the albedo and absorptivity of clouds are prescribed as shown in Table III-2 (here subscript i denotes cloud type). The definitions of u^*_{cT} and u^*_{ci} will be given later.

TABLE III-2. The albedo and absorptivity of clouds. The unit of u^*_{cT} and u^*_{ci} are g cm^{-2}.

Cloud Type i	Scattered part	Absorbed part			
	Albedo (R^1_i)	Albedo (R_i)	Absorptivity (A_i)	u^*_{cT}	u^*_{ci}
High cloud	0.21	0.19	0.04	0.01 ~0.0002	0.04~0.01 (0.03)
Middle cloud	0.54	0.46	0.20	0.1~0.01	3.2~2.4 (3.0)
Low cloud	0.66	0.50	0.30	1~0.1	14~11 (12)
Cb	0.76	0.60	0.30	0.1~0.01	22~20

2. Interaction between cloud layers and solar radiation

For the scattered part ~~(visible radiation)~~ of the solar radiation, molecular scattering in clouds is negligible compared to scattering by water droplets. Absorption by water droplets and water vapor in clouds can be neglected.

For the absorbed part ~~(near infrared radiation)~~ of the solar radiation, scattering by water droplets and absorption by water vapor and droplets in clouds must both be considered. Thus the behavior of the absorbed part in a cloud layer is very complicated. As yet, an analytical solution suitable for the present purpose has not been obtained. Therefore, the absorption and scattering of the absorbed part in a cloud layer are treated separately under the assumptions presented in subsection (iii).

(i) The albedo of a cloudy atmosphere for the ~~scattered part~~ of the solar radiation

Consider a single cloud layer with albedo R' for the scattered part. Since absorption by the cloud is assumed negligible for the scattered part, the transmissivity of the cloud is $(1-R')$. The transmissivity of a cloudless atmospheric column due to Rayleigh scattering is $(1-\alpha_o)$. Thus the transmissivity for the scattered part of the atmosphere with a single cloud layer can be roughly estimated by $(1-R')(1-\alpha_o)$. Then the albedo for the scattered part of the atmosphere with a single cloud layer is

$$\alpha_c = 1 - (1-R')(1-\alpha_o) , \qquad (III.10)$$
$$= R' + \alpha_o - R'\alpha_o .$$

For a partly cloudy sky with cloudiness CL, α_c is modified as follows:

$$\alpha_c = (1-CL)\alpha_o + CL\cdot(R'+\alpha_o-R'\alpha_o) ,$$
$$= \alpha_o + CR'(1-\alpha_o) , \qquad (III.11)$$

where $CR' = CL\cdot R'$. (III.11) is identical to (III.10) with R' replaced by CR'.

(ii) The albedo of multi-layer clouds

(a) 2 cloud layers

Let the albedos of the two cloud layers be R_1' and R_2'. Multiple reflection between the two cloud layers must be considered. As shown schematically in Fig. III-1, the total transmissivity T_{12} is the sum of $T_{12}^{I}, T_{12}^{II}, T_{12}^{III}, \ldots$, where

$$T_{12}^{I} = (1-R_1')(1-R_2') ,$$

$$T_{12}^{II} = (1-R_1')(1-R_2')R_1'R_2' ,$$

$$T_{12}^{III} = (1-R_1')(1-R_2')R_1'^2R_2'^2 .$$

do not add primes on R

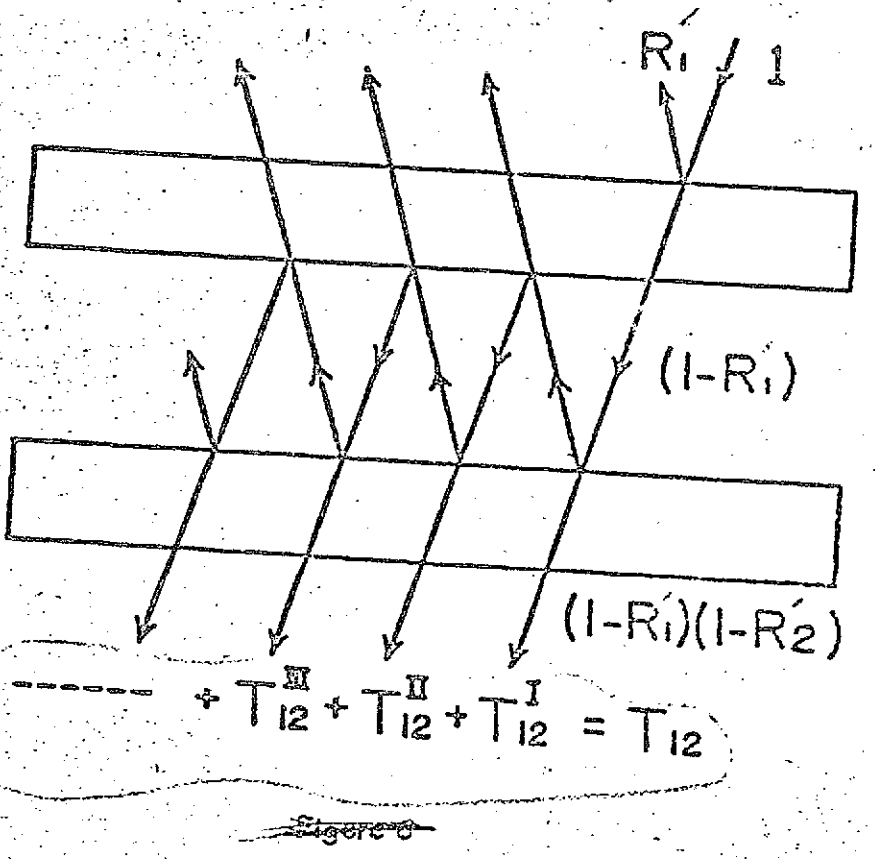

Fig. III-1. Schematic chart for the total albedo of two cloud layers.

Then $$T_{12} = T_{12}^{I} + T_{12}^{II} + T_{12}^{III} + \cdots ,$$

$$= (1-R_1)(1-R_2')[1 + R_1R_2' + (R_1R_2')^2 + \cdots] ,$$

$$= (1-R_1')(1-R_2')/(1-R_1'R_2') \qquad \text{(III.12)}$$

and $$R_{12}' = 1 - T_{12} = 1 - \frac{(1-R_1')(1-R_2')}{1-R_1R_2'} . \qquad \text{(III.13)}$$

(b) 3 cloud layers

Let the albedos of the three cloud layers be R_1', R_2' and R_3'. The total albedo of the 3 cloud layers can be found by considering two cloud layers with albedos R_{12}' and R_3'. Then from (III.13),

$$R_{123}' = 1 - T_{123} ,$$

$$= 1 - \frac{(1-R_{12}')(1-R_3')}{1-R_{12}R_3} ,$$

$$= 1 - \frac{(1-R_1')(1-R_2)(1-R_3')}{1-(R_1R_2+R_2R_3+R_3R_1) + 2R_1R_2R_3} , \qquad \text{(III.14)}$$

(c) Multiple cloud layers

Let the albedos of the n cloud layers be $R_1', R_2', \ldots, R_n'$. Repeating the procedure by which (III.14) was obtained, the following general expression for the total albedo of the n cloud layers is obtained:

$$R_{12\cdots n}' = 1 - E(R_1', \ldots, R_n')/D(R_1', \ldots, R_n') , \qquad \text{(III.15)}$$

where $$E(R_1', \ldots, R_n') = \prod_{i=1}^{n} (1-R_i') ,$$

$$D(R_1', \ldots, R_n') = 1 - \sum_{i<j} R_i'R_j' + 2 \sum_{i<j<k} R_i'R_j'R_k' - 3 \sum_{i<j<k<\ell} R_i'R_j'R_k'R_\ell' + \cdots + (-1)^{n-1}(n-1)R_1'R_2' \cdots R_n' ,$$

and, for example, $\sum_{1 \le i \le n,\ i<j} R_i R_j$ means the summation of all $R_i R_j$ for which $i < j$ and the number of terms is equal to $n \cdot C_2 \to {}_nC_2$.

(iii)

(ii) The equivalent cloud water vapor amount and assumptions for the absorbed part of the solar radiation

The following assumptions are made for the absorbed part of the solar radiation (subscript i denotes cloud type):

(a) The albedo R_i and absorptivity A_i are prescribed as shown in Table III-2.

(b) The albedo of a cloud for the absorbed part results from back scattering by cloud water droplets. This reflected insolation may, before it exits the cloud top, be subject to considerable absorption; however this absorption is neglected.

(c) The absorption of the reflected radiation after it leaves the cloud is neglected.

(d) Solar radiation in a cloud and radiation transmitted by a cloud are diffuse radiation. The effective optical thickness for diffuse radiation is assumed to be 1.66 times the length of a vertical column, that is $\sec \zeta = 1.66$ ($\zeta = 53^\circ$).

(e) The cloud layer is regarded as a fictitious water vapor layer which absorbs the same amount of insolation as that absorbed by the cloud. The water vapor amount of such a fictitious layer is denoted by u^*_{ci}, the equivalent cloud water vapor amount.

Let the effective water vapor amount between the top of the atmosphere and the cloud top be u^*_{cT}. Since the absorbed part of the solar radiation incident on the cloud top is $S^a_o [1 - A(u^*_{cT} \sec \zeta)]$, the total absorption by the cloud is $A_i S^a_o [1 - A(u^*_{cT} \sec \zeta)]$. By assumptions (b) and (e), this total absorption is

equal to the absorption by a fictitious layer of water vapor having an equivalent cloud water vapor amount u_{ci}^*. By assumption (d), the following relation is obtained:

$$A_i S_o^a [1-A(u_{cT}^{*\prime} \sec\zeta)] =$$

$$(1-R_i) S_o^a [A(u_{cT}^{*\prime} \sec\zeta + 1.66\, u_{ci}^*) - A(u_{cT}^{*\prime} \sec\zeta)] . \quad \text{(III.16)}$$

By (III.5), the above relation yields the solution for u_{ci}^*:

$$u_{ci}^* = \left[\left(\frac{A_i[1-A(x)] + (1-R_i)\,A(x)}{0.271\,(1-R_i)}\right)^{3.3} - x\right]/1.66 , \quad \text{(III.17)}$$

where $x = u_{cT}^{*\prime} \sec\zeta$.

Fig. III.2 shows the relation between u_{ci}^* and x for the four combinations of R_i and A_i in Table III-2. The values of u_{ci}^* shown in Table III-2 correspond to the possible range of $u_{cT}^{*\prime}$ with $\sec\zeta = 1$. The values of u_{ci}^* within the parentheses in Table III-2 represent the mean values adopted in the current model.

The above procedure for the estimation of u_{ci}^* is somewhat sophisticated. The values of u_{ci}^* in Table III-2 show only the normal conditions for the four cloud types. If the value of u_{ci}^* is fixed for each cloud type, the absorptivity A_i of a cloud type will change with $u_{cT}^{*\prime}$; an increase of $u_{cT}^{*\prime}$ corresponds to a decrease of A_i. delete

In the current model, a cloud with a temperature less than -40°C is assumed to be a cirrus type cloud. The normal value of u_{ci}^* for cirrus is very small, say 0.03 g cm^{-2}. Thus, when a middle or low cloud is assumed to be cirrus, u_{ci}^* may be smaller than the water vapor amount of the environmental layer. To avoid such an unlikely condition, the fixed value of u_{ci}^* for cirrus

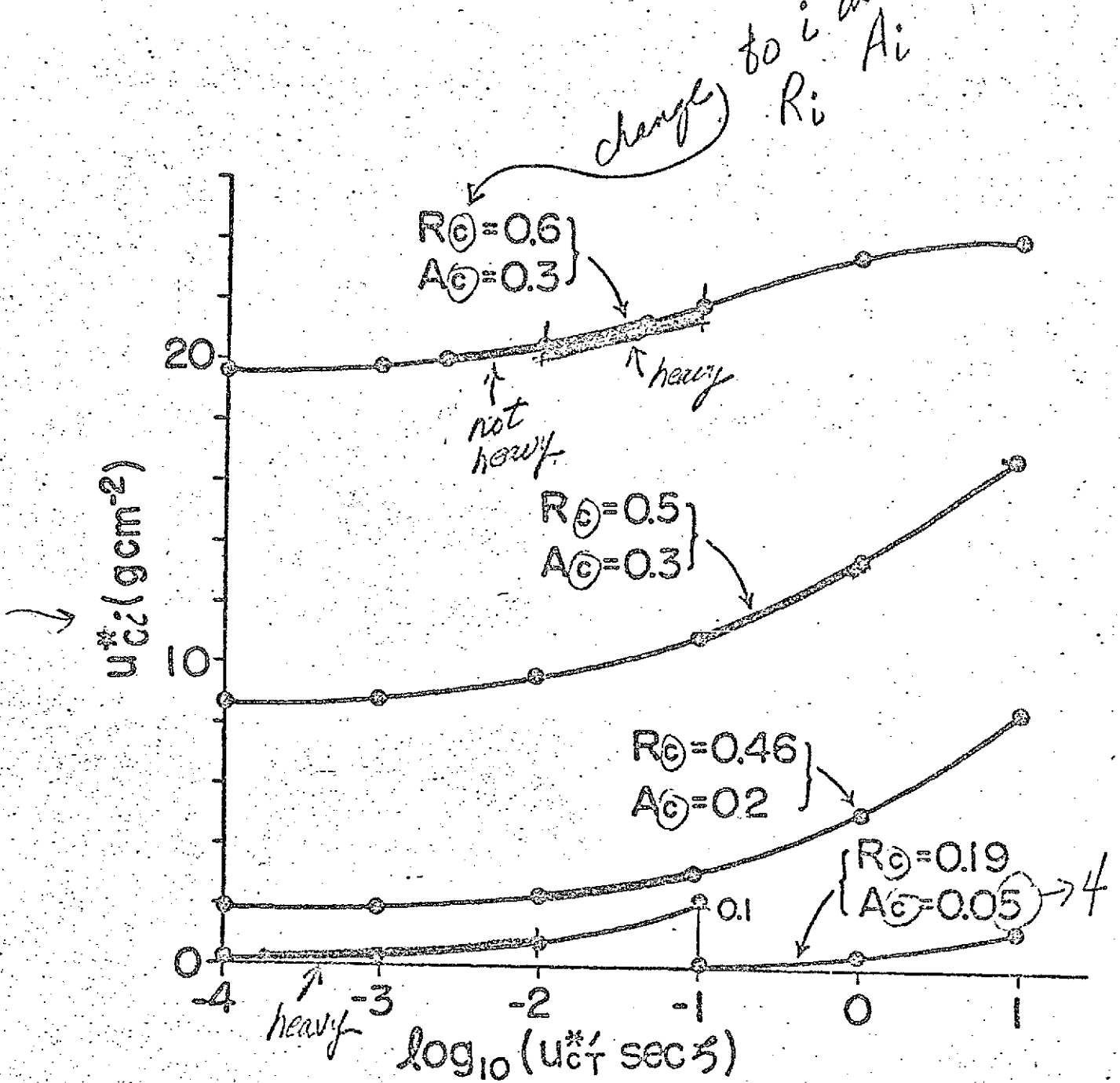

Fig. III-2. The relation . . . . .

~ ~ ~ Figure 7 ~ ~ atmosphere.

(see p. iv)

is modified by adding to it the water vapor amount of the clear area in the corresponding layer.

3. The finite difference scheme for a clear sky

The indexing scheme is shown in Fig. II-2. In the following, superscript o denotes conditions for a clear sky.

The downward flux at level i of the absorbed part of the solar radiation is

$$S^{o}_{ai} = S^{a}_{o} [1-A((u^{*}_{T}-u^{*}_{i}) \sec \zeta)] , \qquad (III.18)$$

where index T denotes the top of the atmosphere. The absorption of solar radiation in the layer between j-1 and j+1, AS^{o}_{j}, is therefore

$$AS^{o}_{j} = S^{o}_{a\,j-1} - S^{o}_{a\,j+1} . \qquad (III.19)$$

The solar radiation reaching the earth's surface is:

The absorbed part: $$S^{o}_{aI} = S^{a}_{o} [1-A(u^{*}_{T} \sec \zeta)] , \qquad (III.20)$$

The scattered part: $$S^{o}_{sI} = S^{s}_{o}(1-\alpha_{o})/(1-\alpha_{o}\alpha_{s}) , \qquad (III.21)$$

where α_s is the surface albedo and the denominator for the scattered part represents the correction factor due to multiple reflection between the atmosphere and the earth's surface. The total solar radiation absorbed by the earth's surface is then

$$S^{o}_{I} = (1-\alpha_{s})[S^{o}_{aI}+S^{o}_{sI}] . \qquad (III.22)$$

4. The finite difference scheme for a cloudy sky

(i) One cloud layer

When the sky is covered by only a single cloud layer, the complex behavior of the solar radiation can be calculated by use of the concept of the equivalent cloud water vapor amount. In the following, superscript c denotes conditions for a cloudy sky.

From the assumptions discussed in sections 2(i) and (iii), the downward flux of the absorbed part of the solar radiation is (see Fig. III-3):

(a) at a level above the cloud

$$S^c_{a_U} = S^a_o \left[1-A\left((u^*_T - u^*_U)\sec\zeta\right)\right] , \qquad \text{(III.23)}$$

(b) at a level within the cloud

$$S^c_{a_M} = S^a_o (1-R_c)\left[1-A\left(X+1.66\,\frac{\Delta p_M}{\Delta p_c}\,u^*_c\right)\right] , \qquad \text{(III.24)}$$

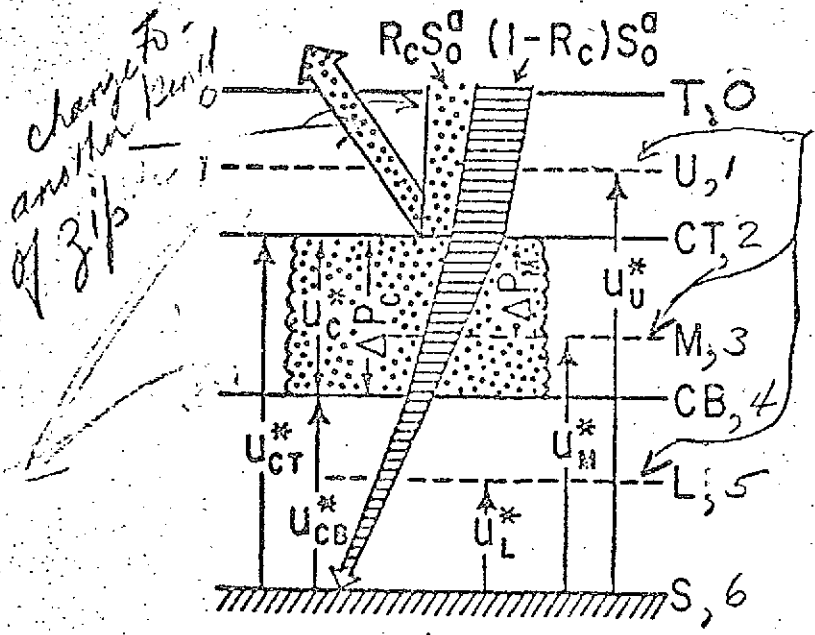

Fig. III-3. Schematic ..... layer.

Figure 8

(c) at a level beneath the cloud

$$S^c_{aL} = S^a_o(1-R_c)[1-A(X+1.66(u^*_c + u^*_{cB} - u^*_L))] \,, \qquad \text{(III.25)}$$

(d) at the cloud top

$$S^c_{acT} = S^a_o[1-A(X)] \,, \qquad \text{(III.26)}$$

where $X \equiv (u^*_T - u^*_{cT})\sec\zeta$. Subscripts U, M and L denote the levels above, within, and beneath the cloud, respectively. Δp_c is the pressure thickness of the layer between CT and M. R_c and u^*_c are used in lieu of R_i and u^*_{ci}, respectively.

The absorption of solar radiation in the layer between j-1 and j+1, SA^c_j is then:

(a) if both levels j-1 and j+1 are above or beneath the cloud top,

$$AS^c_j = S^c_{a\,j-1} - S^c_{a\,j+1} \,, \qquad \text{(III.27)}$$

(b) if level j-1 is above, and level j+1 beneath, the cloud top,

$$AS^c_j = S^c_{a\,j-1} - (S^c_{a\,j+1} + R_c S^c_{acT}) \,, \qquad \text{(III.28)}$$

The last term on the right hand side represents the radiation of the absorbed part reflected at the cloud top.

The solar radiation reaching the earth's surface is divided into the absorbed part S^c_{aI} and the scattered part S^c_{sI}. The absorbed part is given by (III.25) with $u^*_L = 0$. The scattered part is given by (III.21) with α_o replaced by α_c, where by (III.10),

$$\alpha_c = 1-(1-R_c)(1-\alpha_o) \,.$$

The total solar radiation absorbed by the earth's surface is then

$$S^c_I = (1-\alpha_s)[S^c_{aI} + S^c_{sI}] \,, \qquad \text{(III.29)}$$

where

$$S^c_{aI} = S^a_o(1-R_c)[1-A(X+1.66(u^*_c+u^*_{cB}))]/(1-R_c\alpha_s) , \quad \text{(III.30)}$$

$$S^c_{sI} = S^s_o(1-\alpha_c)/(1-\alpha_c\alpha_s) , \quad \text{(III.31)}$$

The denominator of (III.30) is the correction factor due to the multiple reflection between the cloud and the earth's surface.

For a partly cloudy condition with cloudiness CL, the absorption in a reference layer AS_i and at the earth's surface S_I are approximated by

$$AS_i = (1-CL)AS^o_i + CL\cdot AS^c_i , \quad \text{(III.32)}$$

$$S_I = (1-CL)S^o_I + CL\cdot S^c_I . \quad \text{(III.33)}$$

The above single cloud layer model ~~has been employed~~ was used in the UCLA moist 2-layer general circulation model. ~~The~~ A detailed description of the programming ~~is~~ was presented by Gates, et al (1971).

(ii) Multiple cloud layers

The assumptions presented in section II.5 regarding the distribution of cloud layers are again made. Whereas the procedure developed in the preceding subsection (i) applied to quasi-vertical clouds such as cumulonimbus, the following treatment applies to multiple layers of quasi-horizontal clouds.

The indexing scheme is shown in Fig. II-2. Let i and j be ~~even~~ odd and ~~odd~~ even integers, respectively. Layer j means the layer between levels j-1 and j+1.

Define a cloud state index, ℓ_j, which can have only the values 0 and 1. If $\ell_j = 1$ (or 0), the incident solar radiation passes through a cloudy area (or a clear area) in layer j. In an n-layer model, the ~~state index~~ cloud ℓ is an n-dimensional vector,

where $N = 2n-1$.

$(\ell_1, \ldots, \ell_i, \ldots \ell_N)$. If the cloud layers are scattered, there are 2^n different possible cloud states. Fig. III-4 shows the four possible cloud states ℓ for the lower layer of a 2-layer model.

Let the optical path length of the layer between the top of the atmosphere, level T, and a reference level i be denoted by D_{Ti}. Since there are i/2 layers between levels T and i, there are $2^{i/2}$ different possible cloud states for the solar radiation transferred from the top of the atmosphere to level i. Each cloud state corresponds to a different value of D_{Ti}. Let $D_{Ti}(\ell_1, \ell_3, \ldots, \ell_{i-1})$ denote D_{Ti} for the cloud state $(\ell_1, \ell_3, \ldots, \ell_{i-1})$.

that may contain clouds

The optical path length in the layer between levels i-2 and i, $\Delta D_{i-2,i}$, may have three different expressions corresponding to the different cloud states above level i as follows:

(a) when solar radiation passes through a cloud area in the i-1 layer ($\ell_{i-1} = 1$),

$$\Delta D_{i-2,i} = 1.66\, u^*_{cj\,i-1} \quad (III.34)$$

(b) when solar radiation does not pass through any cloud area in the layers above level i ($\ell_j = 0,\ 1 \le j \le i-1$),

$$\Delta D_{i-2,i} = (u^*_{i-2} - u^*_i) \sec\zeta \quad (III.35)$$

(c) when solar radiation passes through a cloud area in any layer above level i-2 and passes through a clear area in layer i-1 (one or more of the ℓ_j for $1 \le j \le i-3$ has a value of 1 and $\ell_{i-1} = 0$),

$$\Delta D_{i-2,i} = 1.66\,(u^*_{i-2} - u^*_i) \quad (III.36)$$

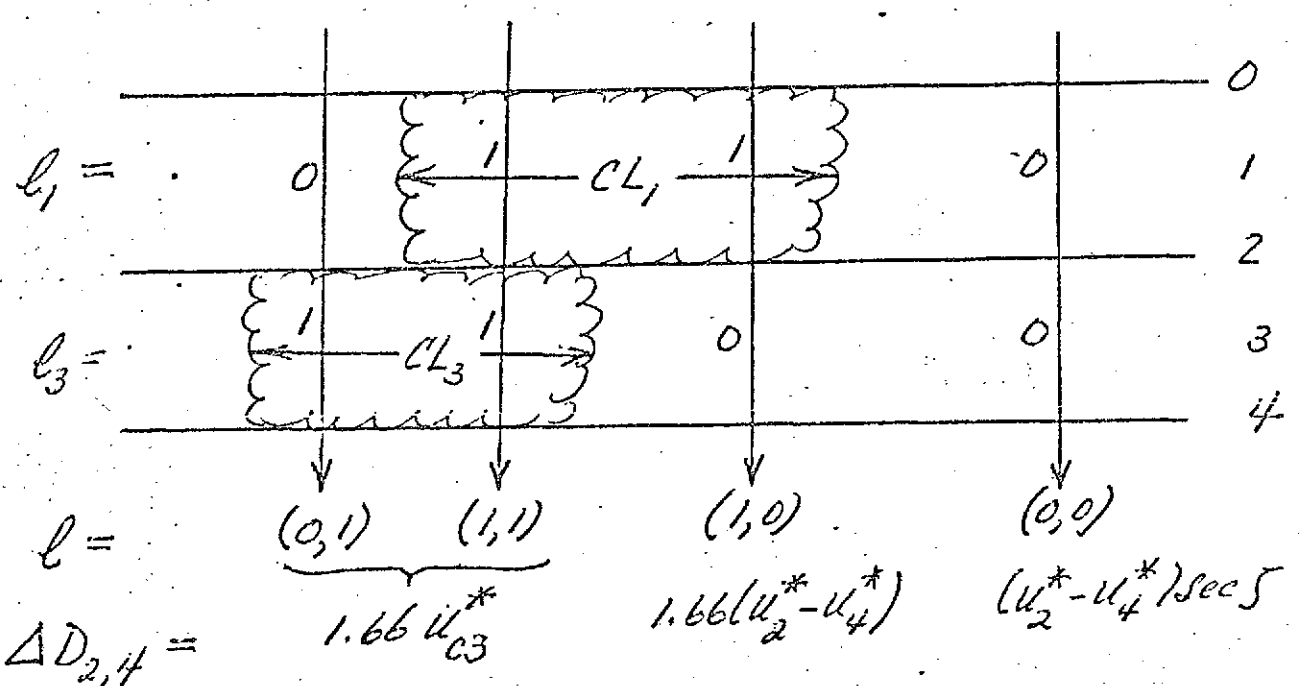

Fig. III-4. Cloud state indices ℓ_1 and ℓ_3, the four possible cloud states ℓ for the lower layer and ~~the~~ ~~corresponding~~ ~~four~~ ~~three~~ the three possible optical path lengths ~~four~~ $\Delta D_{2,4}$ for the lower layer of a 2-layer model.

Defining

$$M_i = \begin{cases} 1 & \text{for } i < 4 \\ \prod_{j=1}^{i-3} (1-\ell_j) & \text{for } i \geq 4 \end{cases} \quad (III.37)$$

the cloud state for the three cases above can be classified as

(a) $\ell_{i-1} = 1$

(b) $\ell_{i-1} = 0, \quad M_i = 1$

(c) $\ell_{i-1} = 0, \quad M_i = 0$.

The general expression for $\Delta D_{i-2,i}$ is then

$$\Delta D_{i-2,i} = 1.66\, u^*_{c,i-1}\, \ell_{i-1} + (u^*_{i-2} - u^*_i)\,[M_i \sec\zeta + 1.66(1-M_i)](1-\ell_{i-1}) \quad (III.38)$$

D_{Ti} for a cloud state $(\ell_1, \ldots, \ell_{i-1})$ is

$$D_{Ti}(\ell_1, \ldots, \ell_{i-3}, \ell_{i-1}) = D_{T,i-2}(\ell_1, \ldots, \ell_{i-3}) + \Delta D_{i-2,i} \quad (III.39)$$

For example, D_{Ti} at levels 0, 2 and 4 ~~are~~ of a 2-layer model are (see Fig. III-4)

$$\begin{aligned} D_{T0} &= (u^*_T - u^*_0) \sec\zeta \\ D_{T2}(0) &= D_{T0} + (u^*_0 - u^*_2) \sec\zeta \\ D_{T2}(1) &= D_{T0} + 1.66\, u^*_{c1} \end{aligned} \quad (III.40)$$

$$\begin{aligned} D_{T4}(0,0) &= D_{T2}(0) + (u^*_2 - u^*_4) \sec\zeta \\ D_{T4}(0,1) &= D_{T2}(0) + 1.66\, u^*_{c3} \\ D_{T4}(1,0) &= D_{T2}(1) + 1.66\,(u^*_2 - u^*_4) \\ D_{T4}(1,1) &= D_{T2}(1) + 1.66\, u^*_{c3} \end{aligned} \quad (III.41)$$

Let the fractional area occupied by a cloud state $(\ell_1, \ldots, \ell_n)$ be denoted by $W(\ell_1, \ldots, \ell_n)$. Assuming that all cloud layers are horizontally quasi-homogeneous,

$$W(\ell_1, \ldots, \ell_n) = \prod_{j=1}^{n} w(\ell_j) \quad , \tag{III.42}$$

where

$$w(\ell_j) = (1-\ell_j)(1-CL_j) + \ell_j CL_j \quad , \tag{III.43}$$

and CL_j is the cloudiness of layer j. W has the property that $\sum W(\ell_1, \ldots, \ell_n) = 1$, where the summation is taken over all possible cloud states. For example, for a 2-layer model,

$$W(0,0) = (1-CL_1)(1-CL_3) \quad ,$$
$$W(0,1) = (1-CL_1)CL_3 \quad ,$$
$$W(1,0) = CL_1(1-CL_3) \quad ,$$
$$W(1,1) = CL_1 \cdot CL_3 \quad ,$$

and $W(0,0) + W(0,1) + W(1,0) + W(1,1) = 1$.

If the insolation incident at the top of layer j meets a cloud area, a fraction R_j is reflected back. It is therefore useful to define another weighting function $W'(\ell_1, \ldots, \ell_n)$ such that reflection is taken into account, namely

$$W'(\ell_1, \ldots, \ell_n) = \prod_{j=1}^{n} w'(\ell_j) \quad , \tag{III.44}$$

where

$$w'(\ell_j) = w(\ell_j)[(1-\ell_j) + \ell_j(1-R_j)] \quad ,$$
$$= (1-\ell_j)(1-CL_j) + \ell_j CL_j(1-R_j) \quad . \tag{III.45}$$

The last expression was obtained via the relation $\ell_j^2 = \ell_j$, $(1-\ell_j)^2 = (1-\ell_j)$, and $\ell_j(1-\ell_j) = 0$. $W'(\ell_1, \ldots, \ell_N)$ represents the transmissivity-weighted fractional area occupied by the cloud state $(\ell_1, \ldots, \ell_N)$.

Let the total albedo for both the scattered part of the radiation and the fraction of the absorbed part that is reflected by clouds be, for a cloud

change n to N

state $(\ell_1, \ldots, \ell_{(n)})$, $R(\ell_1, \ldots, \ell_{(n)})$. By (III-15), with R_i replaced by $\ell_i R_i$,

$$R(\ell_1, \ldots, \ell_{(n)}) = 1 - [E(\ell_1 R_1, \ldots, \ell_{(n)} R_{(n)}) / D(\ell_1 R_1, \ldots, \ell_{(n)} R_{(n)})] \,. \qquad \text{(III.46)}$$

Thus, for example, $R(1,1) = R_{13}$, $R(0,1,0) = R_3$, $R(1,1,1) = R_{135}$ and $R(0,0,0) = 0$.

The radiation budgets for an atmospheric layer and at the earth's surface can now be formulated on the basis of the above results.

Absorption in an atmospheric layer

The downward flux of the absorbed part of the solar radiation at levels i and i+2 can be expressed as

$$S_{ai} = S_o^a \sum^{m_i} W'(\ell_1, \ldots, \ell_{i-1})[1 - A(D_{Ti}(\ell_1, \ldots, \ell_{i-1}))] \,, \qquad \text{(III.47)}$$

$$S_{a\,i+2} = S_o^a \sum^{m_{i+2}} W'(\ell_1, \ldots, \ell_{i-1}, \ell_{i+1})[1 - A(D_{T\,i+2}(\ell_1, \ldots, \ell_{i-1}, \ell_{i+1}))] \,, \qquad \text{(III.48)}$$

where the summation is taken over all the $m_i = 2^{i/2}$ different possible cloud states. Since the net downward flux through level i of the absorbed part of the radiation is $(1 - R_{i+1})S_{ai}$, the absorption in layer i+1 is

$$AS_{i+1} = (1 - R_{i+1})S_{ai} - S_{a\,i+2} \,. \qquad \text{(III.49)}$$

CL$_{i+1}$

Absorption by the earth's surface

The absorbed part of the solar radiation that reaches the earth's surface is estimated by (III.47) as

$$S'_{aI} = S_o^a \sum^{m_I} W'(\ell_1, \ldots, \ell_{I-1}) \left[\frac{1 - A(D_{TI}(\ell_1, \ldots, \ell_{I-1}))}{1 - a_s R(\ell_1, \ldots, \ell_{I-1})} \right] , \qquad \text{(III.50)}$$

where the denominator is the correction factor due to multiple reflection between the clouds and the earth's surface. However, in addition to S'_{aI}, some fraction of the absorbed part of the solar radiation that is reflected at the tops of clouds

can reach the earth's surface after multiple reflections between cloud layers.

Let the contribution to the downward insolation at the surface from radiation reflected at level i (and subsequently multiply-reflected between cloud layers) be S^i_{aI}. Let R_U and R_L be the total albedos of the cloud groups above and below level i and let the total albedo of all the cloud groups in the entire atmosphere be R_{U+L}. The absorbed part of the solar radiation reflected at level i is $S_{ai}R_{i+1}$. After multiple reflections between the upper and lower cloud groups, the fraction $R_U/(1-R_U R_L)$ has been scattered back to level i as a downward flux. Of this, the fraction $(1-R_L)$ is transmitted through the lower cloud group to reach the earth's surface. Multiple reflections between the earth's surface and all the cloud groups can be introduced via the factor $1/(1-R_{U+L}\alpha_s)$.

If the i+1 layer is devoid of clouds, reflection at level i does not occur. Consideraing this fact, S^i_{aI} for a cloud state $(\ell_1, \ldots, \ell_{I-1})$ is given by

$$S^i_{aI}(\ell_1, \ldots, \ell_{I-1}) = S_{a\ell_{i+1}} R_{i+1} R_U (1-R_L)/[(1-R_U R_L)(1-R_{U+L}\alpha_s)] , \qquad \text{(III.51)}$$

where

$$R_U = R(\ell_1, \ldots, \ell_{i-1}) ,$$

$$R_L = R(\ell_{i+1}, \ldots, \ell_{I-1}) ,$$

$$R_{U+L} = R(\ell_1, \ldots, \ell_{I-1}) ,$$

and

$$S^i_{aI} = \sum^{m^I} W(\ell_1, \ldots, \ell_{I-1}) S^i_{aI}(\ell_1, \ldots, \ell_{I-1}) , \qquad \text{(III.52)}$$

Finally, the absorbed part of the solar radiation that reaches the earth's surface is

$$S'_{aI} + \sum_{i=2}^{I-1} S^i_{aI} , \qquad \text{(III.53)}$$

Since different values are adopted for the albedos of the scattered and absorbed parts of the solar radiation, let R'_i and $R'(\ell_1, \ldots, \ell_n)$ denote the former and R_i and $R(\ell_1, \ldots, \ell_n)$ denote the latter.

In analogy to (III.30) and (III.21), the scattered part of the solar radiation that reaches the earth's surface is

$$S_{sI} = S_o^s \sum^{m_I} W(\ell_1, \ldots, \ell_{I-1}) \left[\frac{1-\alpha_c(\ell_1, \ldots, \ell_{I-1})}{1-\alpha_s \alpha_c(\ell_1, \ldots, \ell_{I-1})} \right] , \qquad \text{(III.54)}$$

where

$$\alpha_c(\ell_1, \ldots, \ell_{I-1}) = 1-(1-\alpha_o)[1-R'(\ell_1, \ldots, \ell_{I-1})] . \qquad \text{(III.55)}$$

Finally, the total absorption of the earth's surface of both the scattered and absorbed part of the solar radiation is

$$S_I = (1-\alpha_s)(S'_{aI} + \sum_{i=2}^{I-2} S^i_{aI} + S_{sI}) . \qquad \text{(III.56)}$$

The symbolic expressions developed in this section for multiple cloud layers appear to be relatively simple. However, the complexity and computer time requirement of the computation increase very rapidly with increasing vertical resolution. Therefore, it may be advantageous to introduce the following simplifications into the model.

(a) No overlapping cloud layers.

Overlapping of cloud layers is prohibited; at most, only one of the ℓ_j's is equal to one. Thus, for an n-layer model, there are only $n+1$ different possible cloud states $(\ell_1, \ldots, \ell_n)$. This simplification reduces the computation to a superposition of single cloud layers.

(b) No partly cloudy condition.

The cloudiness is restricted to either 0 or 1; ℓ_i in any layer can have only a single value. Thus, at any time and position, there is only a single cloud state $(\ell_1, \ldots, \ell_n)$. → N

The radiation scheme for the current UCLA 3-layer GCM has been formulated with ~~the above simplifications~~. As shown in Appendix B, the scheme is relatively straightforward. → simplification (b).

5. Surface albedo

The earth's surface is divided into three categories: sea surface, snow-free land, and snow and ice surfaces. 2/5.

i) Sea surface

The albedo of the sea surface is a function of the overlying cloud condition, the solar zenith angle, and the wave state of the sea surface.

Under a clear sky, a majority of the solar insolation reaches the earth's surface as direct radiation. The albedo of a smooth sea surface for direct radiation increases from a few per cent to about 100 per cent as the solar zenith angle increases. Since the mean solar zenith angle increases with latitude, the albedo of the sea surface is usually somewhat larger in high latitudes than in low latitudes.

Under an overcast sky, almost all of the solar insolation reaches the surface as diffuse radiation. The albedo of the sea surface for diffuse radiation is nearly a constant value of 0.07.

In the present 3-layer GCM, a constant value of 0.07 is adopted as the sea surface albedo.

(ii) Snow-free land

The albedo of snow-free land depends upon the soil condition (especially color) and the extent and color of natural vegetation. Coniferous forests with dark leaves have an albedo of about 0.14 while deserts covered by light colored sand have an albedo larger than 0.3. Seasonal variations in albedo caused by leaves withering or turning yellow are not uncommon.

It appears that the spatial and seasonal changes in albedo are not essential to the simultation of the general circulation. Therefore, following Posey and Clapp (1964), a constant albedo of 0.14 is adopted for snow-free land.

(iii) Snow and ice

The albedo of snow and ice varies considerably with their cyrstalline structure. The latter is a function of temperature and, in the case of snow, age. Thus, the albedo of snow depends upon whether the snow is wet or dry, fresh or old, and whether or not it is in the melting stage. The albedo of ice depends upon whether ~~the ice~~ it is sea pack ice or permanent land ice, and whether or not it is in the melting stage.

In "Climates of the Polar Regions" (edited by Orvig, 1970), Putniss, Vowinckel and Orvig, and Schwerdtfeger discuss the albedo of the snow and ice surfaces of Greenland, the North Polar Basin, and Antarctica, respectively. Their key results are:

(a) the albedo of snow varies from 55% to 100%,
(b) the albedo of sea ice varies from 20% to 60%,
(c) the albedo of permanent snow and ice fields over the interior of land has a lower limit of about 80%.

In addition, the albedo of snow-covered land may vary considerably with the type of underlying surface. For example, the albedo of a snow-covered forest area depends upon the type of forest, the density of trees and the depth of the snow cover.

In midsummer, the ice and snow surfaces of the polar region receive more than 700 ly day^{-1} of solar radiation. If the surface albedo changes by 0.1, the solar radiation absorbed by a surface changes by more than 70 ly day^{-1}; this amount is of the same order as the net outgoing long wave radiation from the earth's surface. Therefore, in midsummer, the radiation budget at the polar regions is very sensitive to the surface albedo. Since the albedos of snow and ice surfaces may vary from 0.2 to 1.0, special attention must be paid to the prescription of the surface albedo for the summer polar region.

In the current 3-layer model, albedos of 0.4 for sea ice and 0.7 for snow have been adopted. For permanent ice and snow fields over land interiors, Min(0.85, 0.7+0.00015 h) has been employed, where h is the land surface elevation in meters.

In summary, in the current UCLA 3-layer GMC, the assumed values of surface albedo α_s are:

Surface	Albedo, α_s
snow-free land	0.14
sea	0.07
sea ice	0.4
temporary snow	0.7
permanent land ice and snow	Min(0.85, 0.7 +0.00015 h)

IV. VERTICAL DISTRIBUTION OF WATER VAPOR AND CARBON DIOXIDE

1. Water vapor

The effective water vapor amount in an air column of height z, u_z^*, can be obtained from equation (II.3) if the vertical distribution of water vapor mixing ratio q is known. In principle, since the UCLA 3-layer GCM predicts q for each layer from the moisture conservation equation, u_z^* for each level in the troposphere could be estimated straightforwardly from (II.3). However, for simplicity, an assumed vertical distribution of q will be employed rather than that predicted by the GCM. Smith (1966) has shown that the climatic value of the mixing-ratio in the lower troposphere can be expressed by

$$q \propto p \qquad \text{(IV.1)}$$

Two methods, based upon different forms of this relation for the entire troposphere, will be developed subsequently.

Although the present UCLA 3-layer GCM does not predict the water vapor content in the stratosphere, this quantity is necessary for the radiation calculation. Aircraft observations by the British group (for example, Murgatroyd et al (1955)) have shown that the frost-point temperature decreases rapidly near the tropopause and tends to asymptotically approach a constant value of about 190°K in the lower stratosphere. Manabe and Möller (1961) summarized the results obtained by the British group and showed that the frost-point temperature in the lower stratosphere could be assumed to be 190°K, irrespective of latitude and season. This assumption was employed in the UCLA 2-layer moist model.

More recently, Williamson and Houghton (1965) estimated from radiometer measurements that the stratospheric mixing ratio is in the neighborhood of 3×10^{-6} g/g at least to 25 km. Mastenbrook (1968), employing balloon-borne frost-point hygrometers, measured the water vapor in the stratosphere over Trinidad, Washington, D.C., and Thule, Greenland during 1964 and 1965. He found that the median vertical distribution of water vapor in the stratosphere to

a height of 28 km, ~~(100 mb, — 15 km)~~ approximates a constant mixing ratio within the range ~~2×10^{-6} — 3×10^{-6} g/g~~ 2×10^{-6} to 3×10^{-6} g/g.

McKinnon and Morewood (1970) also measured the water vapor distribution in the upper troposphere and lower stratosphere from 70°N to 40°S over North and South America by an automatic tracking solar spectrometer mounted in a jet aircraft. They found that the seasonal variations were within a few per cent in the lower stratosphere and that median values above 17.7 km, during Northern Hemisphere winter, gradually decrease from 1.75×10^{-6} at 65°N to 1.25×10^{-6} at 30°S. These values are roughly half those obtained by Mastenbrook and Williamson and Houghton. ~~Therefore,~~ In the current UCLA 3-layer GCM, a constant mixing ratio of 2.5×10^{-6} g/g is assumed for the stratosphere above 100 mb.

(New paragraph)

Although relation (IV.1) is adopted as the vertical distribution of the mixing ratio in the troposphere, there are many possible methods by which q can be estimated from (IV.1). In the following, two methods suitable for the 3-layer GCM ~~will be~~ are presented.

(i) Method A

Throughout the troposphere, the vertical distribution of q is assumed to be expressed by (IV.1) with a single value of k. Thus

$$q = \begin{cases} q_{ST} (p/p_{ST})^k & \text{for } p > p_{ST} = 100 \text{ mb} \\ q_{ST} = 2.5 \times 10^{-6} & \text{for } p \le p_{ST} \end{cases} \quad \text{(IV.2)}$$

By (II.3), the effective water vapor amount of $p_z \ge p_{ST}$ is

$$u^* = \frac{\beta}{\gamma}\left[\left(\frac{p_g}{p_{ST}}\right)^\gamma - \left(\frac{p_z}{p_{ST}}\right)^\gamma\right] \quad \text{(IV.3)}$$

where $\beta = p_{ST}^{\alpha+1} q_{ST} / g p_{\infty}^{\alpha} = 2.551 \times (0.1)^{\alpha} \times 10^{-4}$ (cm)

$\gamma = k + \alpha + 1$

and for $p_{(z)} \leq p_{ST}$,

$$u^*_{(z)} = u^*_{ST} + \frac{\beta}{\alpha+1}\left[1 - \left(\frac{p_{(z)}}{p_{ST}}\right)^{\alpha+1}\right], \qquad \text{(IV.4)}$$

where u^*_{ST} means u^* for $p_{(z)} = p_{ST}$.

It is now necessary to estimate a value of k at each grid point. From (IV.2),

$$\log(q/q_{ST}) = k \log(p/p_{ST}) \qquad \text{(IV.5)}$$

The simplest way to obtain a single value of k for an N-layer tropospheric model may be

$$k = \sum_{j=1}^{N} \log(q_j/q_{ST}) \Big/ \sum_{j=1}^{N} \log(p_j/p_{ST})$$

$$= \log\left(\prod_{j=1}^{N}(q_j/q_{ST})\right) \Big/ \log\left(\prod_{j=1}^{N}(p_j/p_{ST})\right) \qquad \text{(IV.6)}$$

where $M = 2N-1$.

For a 3-layer model, (IV.6) becomes

$$k = \log(q_1 \cdot q_3 \cdot q_5 / q_{ST}^3) / \log(p_1 \cdot p_3 \cdot p_5 / p_{ST}^3) \qquad \text{(IV.7)}$$

However, if a least squares method is used,

$$k = \sum_{j=1}^{N} \log(q_j/q_{ST}) \cdot \log(p_j/p_{ST}) \Big/ \sum_{j=1}^{N} \log^2(p_j/p_{ST}) \qquad \text{(IV.8)}$$

This expression may be superior to (IV.6) but it also requires much more computer time.

If p_j is larger than 400 mb, the range of change of $\log(p_j/p_{ST})$ is less than that of $\log(q_j/q_{ST})$. If $\log(p_j/p_{ST})$ is replaced in (IV.8) by some mean value, (IV.8) reduces to (IV.6) as a limiting case.

(ii) Method B

Two values of k are used to express the vertical distribution of mixing ratio in the troposphere. That is

$$q = q_c (p/p_c)^{k_1} \qquad \text{for } p \geq p_c \,, \tag{IV.9}$$

$$q = q_{ST} (p/p_{ST})^{k_2} \qquad \text{for } p_{ST} \leq p < p_c \,, \tag{IV.10}$$

$$q = q_{ST} = 2.5 \times 10^{-6} \qquad \text{for } p \leq p_{ST} = 100 \text{ mb} \,,$$

where p_c is a critical level in the middle troposphere around 400 mb.

In this case, the effective water vapor amount can be expressed as follows:

$$u^*_{(z)} = \frac{\beta_1}{\gamma_1}\left[\left(\frac{p_g}{p_c}\right)^{\gamma_1} - \left(\frac{p_{(z)}}{p_c}\right)^{\gamma_1}\right] \qquad \text{for } p_{(z)} \geq p_c \,, \tag{IV.11}$$

$$u^*_{(z)} = u^*_c + \frac{\beta_2}{\gamma_2}\left[\left(\frac{p_c}{p_{ST}}\right)^{\gamma_2} - \left(\frac{p_{(z)}}{p_{ST}}\right)^{\gamma_2}\right] \qquad \text{for } p_{ST} < p_{(z)} \leq p_c \,, \tag{IV.12}$$

$$u^*_{(z)} = u^*_{ST} + \frac{\beta_2}{\alpha+1}\left[1 - \left(\frac{p_{(z)}}{p_{ST}}\right)^{\alpha+1}\right] \qquad \text{for } p \leq p_{ST} \,, \tag{IV.4}$$

where

$$\beta_1 = p_c^{\alpha+1} q_c / g\, p_{oo}^{\alpha} \,,$$

$$\gamma_1 = k_1 + \alpha + 1 \,,$$

$$\beta_2 = p_{ST}^{\alpha+1} q_{ST} / g\, p_{oo}^{\alpha} \,,$$

$$\gamma_2 = k_2 + \alpha + 1 \,.$$

To obtain k_1 and q_c, the least squares method is applied to the relation

$$y_j = a + k_1 x_j \,,$$

where $x_j = \log(p_j/p_c)$, $y_j = \log q_j$, $a = \log q_c$.

Then,

$$k_1 = \left(N \sum_{j=1}^{N} x_j y_j - \sum_{j=1}^{N} x_j \sum_{j=1}^{N} y_j\right)/D \qquad \text{(IV.13)}$$

$$q_c = \exp\left(\left(\sum_{j=1}^{N} y_j \sum_{j=1}^{N} x_j^2 - \sum_{j=1}^{N} x_j y_j \sum_{j=1}^{N} x_j\right)/D\right) \qquad \text{(IV.14)}$$

$$D = N \sum_{j=1}^{N} x_j^2 - \left(\sum_{j=1}^{N} x_j\right)^2 .$$

Using the above value of q_c, k_2 is obtained from

$$k_2 = \log(q_c/q_{ST})/\log(p_c/p_{ST}) \qquad \text{(IV.15)}$$

The results of the three methods for estimating k, (IV.6) and (IV.8) of method A, and (IV.13) of method B, will now be compared to observations. Rodgers (1967) presented the zonal mean values of the mixing ratio in the lower troposphere for the northern hemisphere which ~~Rasmuson~~ Rasmusson calculated on the basis of the five year data sample of the MIT General Circulation Library. The values of the mixing ratio were given at 400, 500, 700, 850 and 1000 mb. The seasonal and latitudinal ~~mean values~~ variation of k and the mixing ratio at 1000 mb estimated by the three methods, and the 1000 mb observations, are ~~contrasted~~ compared in Table IV-1. For method B, k_1 and k_2 are shown by numbers without and with parentheses, corresponding to values for the lower troposphere from 1000 mb to 400 mb and for the upper troposphere from 400 mb to 100 mb, respectively (p_c = 400 mb).

With the exception of the lowest layer in the winter high latitudes where an inversion layer predominates, the form of relation (IV.1) is in fairly good agreement with the climatological data in the lower troposphere below 400 mb. It can be considered that k_1 deduced by method B faithfully yields the actual condition for the lower troposphere. Throughout the year, k_1 is larger in midlatitudes than in the tropics and high latitudes and, with the exception of high latitudes, is larger in winter than in summer.

The vertical profiles of the mixing ratio obtained by methods A and B are compared to the observations in Figure IV-1

see p. vii

TABLE IV.1 Seasonal and latitudinal variation of the zonal mean values of k in the troposphere and the mixing ratio at 1000 mb estimated by the three methods. The Method B yields two values of k(k_1 and k_2). The values for the upper troposphere between 100 and 400 mb, k_2, are shown in parentheses.

LAT. (°N)	k			Q 1000 mb (g/Kg)			
	A	A'	B: k_1 k_2	A	A'	B	OBS.
January							
0	3.90	3.93	2.86 (4.31)	19.9	21.3	13.6	13.8
20	3.65	3.65	3.59 (3.67)	11.1	11.1	10.9	10.4
40	3.26	3.26	3.36 (3.22)	4.6	4.6	4.7	4.4
60	2.85	2.84	2.90 (2.82)	1.8	1.7	1.8	1.5
70	2.65	2.65	2.39 (2.75)	1.1	1.1	1.0	0.8
April							
0	3.92	3.95	3.06 (4.26)	20.8	22.3	15.2	14.9
20	3.72	3.72	3.70 (3.73)	13.1	13.1	13.0	12.1
40	3.42	3.43	3.23 (3.50)	6.6	6.7	6.2	5.9
60	3.04	3.05	2.89 (3.10)	2.8	2.8	2.6	2.5
70	2.77	2.77	2.89 (2.72)	1.5	1.5	1.5	1.2
July							
0	4.04	4.08	2.71 (4.57)	27.3	30.1	16.9	16.8
20	3.98	4.02	2.92 (4.40)	24.0	26.2	16.3	16.0
40	3.81	3.83	3.09 (4.09)	16.0	16.7	12.3	12.0
60	3.59	3.60	3.19 (3.74)	9.7	10.0	8.4	7.5
70	3.46	3.47	3.23 (3.55)	7.2	7.4	6.6	6.0
October							
0	4.02	4.06	2.66 (4.55)	26.0	28.7	15.9	16.2
20	3.90	3.92	3.15 (4.20)	19.8	20.8	15.1	14.6
40	3.54	3.55	3.25 (3.66)	8.7	8.9	7.8	7.5
60	3.17	3.17	3.12 (3.19)	3.7	3.7	3.6	3.2
70	3.01	3.02	2.70 (3.13)	2.5	2.6	2.2	2.0

The value of k obtained by method A shows a simpler seasonal and latitudinal variation. Since k is directly proportional to the mixing ratio in the lower troposphere, k decreases with increasing latitude and from summer to winter. This behavior does not agree with the observations.

In low latitudes throughout the year, and in midlatitudes in summer, method A overestimates k by about 1.0. As a result, the mixing ratio at 1000 mb is more than 30 percent larger than the observations. As an extreme case, the solid and dashed curves on the right side of Fig. IV-1 demonstrate the difference between the vertical profiles of the mixing ratio obtained by method A and B, respectively, for the normal condition at the equator in July. The mixing ratio in the lowest 350 mb layer is overestimated, and that in the upper troposphere is underestimated, by method A. This may lead to an overestimation of the cooling rate rate of the tropospheric column by long wave radiation by yielding a too small net upward flux at the earth's surface and a too large net outgoing flux at the top of the troposphere.

Table IV-1 also shows the difference between k deduced by (IV.6) and (IV.8) of method A. The numbers labeled by A' and A refer to (IV.6) and (IV.8), respectively. Since 400 mb is the highest level for which there are observed values of q, as previously discussed, the difference between the A' and A values is negligibly small and (IV.6) can be employed in lieu of (IV.8).

Prior to September, 1971, (IV.6) of method A has been employed in the UCLA 3-layer GCM. Method B is currently undergoing testing prior to its utilization.

more figures to follow Table IV-1

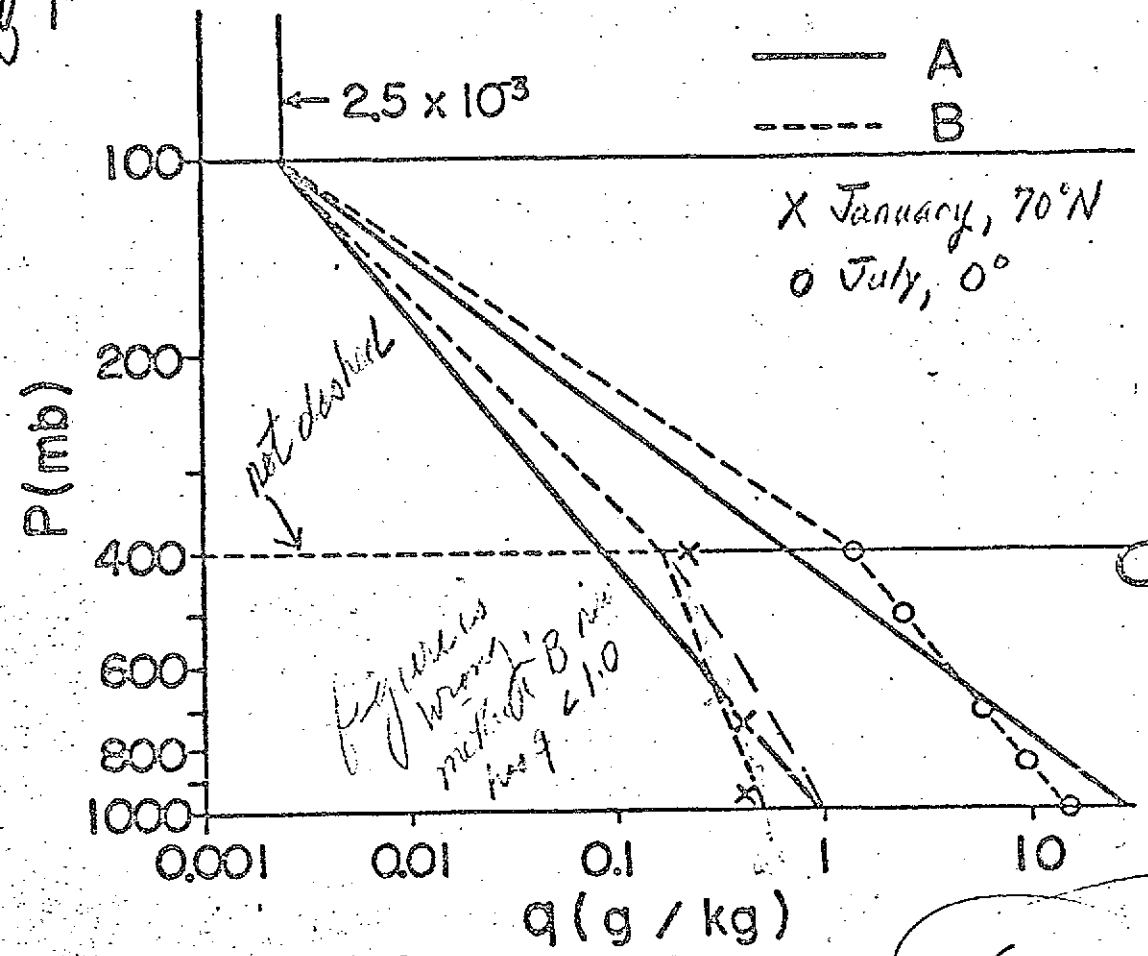

Fig IV-1. Figure 2

(see p. V) for title

(iii) Hemispheric mean normal values of mixing ratio

In order to save computer time, it may be desirable to approximate the interpolation factor m, discussed in section II.2, by constant values over the global domain or throughout the year. Appropriate constant values of m can be obtained by substituting mean values of the mixing ratio into (II.24) - (II.27). For this purpose, Table IV-2 presents the mean normal mixing ratio averaged over the northern hemisphere (0°-70°N) based on Rasmusson's data. Since the semi-empirical expressions for m are functions of log q, the hemispheric mean values shown as $\bar{q}$ represent the mean taken with respect to log q. The constants that are deduced via methods A and B are also shown.

TABLE IV.2. The northern hemisphere mean normal values of mixing ratio $\bar{q}$ and its various constants obtained by methods A and B. The mixing ratio is shown in units of g/kg.

		JAN	APR	JUL	OCT	ANN
$\bar{q}$	1000 mb	6.0	7.6	13.0	9.3	8.6
	850	3.9	4.9	8.4	6.1	5.6
	700	2.0	2.6	4.8	3.3	3.0
	500	0.69	0.86	1.8	1.2	1.1
	400	0.31	0.38	0.85	0.58	0.49
B	k_1	3.24	3.28	2.98	3.06	3.14
	k_2	3.51	3.66	4.23	3.94	3.83
	q_{400}	0.32	0.40	0.88	0.59	0.51
	q_{1000}	6.32	8.05	13.49	9.70	9.03
A	k	3.44	3.56	3.90	3.71	3.65

The annual mean vertical profile of the mixing ratio of water vapor in the troposphere as obtained from method B is

$$q = \begin{cases} 0.51 \times 10^{-3} \left(\frac{p}{400}\right)^{3.14} = 9.03 \times 10^{-3} \left(\frac{p}{1000}\right)^{3.14} & \text{for } p \geq 400 \text{ mb} \\ 2.5 \times 10^{-6} \left(\frac{p}{100}\right)^{3.83} & \text{for } 400 \text{ mb} \geq p \geq 100 \text{ mb}. \end{cases} \quad \text{(IV.16)}$$

(iv) Pressure scaling factor

To evaluate the effective water vapor amount, the pressure scaling factor a must be specified in (II.3).

Elsasser (1942), on the basis of theoretical and laboratory experiments studies, adopted a value of $\alpha = 0.5$ for his radiation chart. Yamamoto (1952) recommended $\alpha = 1.0$ on the basis of studies presented after Elsasser's paper. Based on the laboratory experiment by Howard, et al (1955), Manabe and Möller (1961) adopted $\alpha = 0.6$.

Water vapor has many absorption bands in the infra-red spectral region. Each band consists of many lines whose individual shapes can be important to the radiation transfer computation.

Consider a single absorption line. For a weak line whose center is not blacked out, the total absorption does not depend on pressure broadening, hence $\alpha = 0$. For a strong line whose center region is completely blacked out, theory shows that the total absorption is proportional to the pressure, that is, $\alpha = 1$.

In the actual atmosphere, absorption by water vapor occurs via an ensemble of weak, intermediate and strong lines, and the fractional percentage of each line changes with the amount of the absorber. Therefore, the value of α may vary from 0 to 1, depending upon atmospheric conditions.

In the lower troposphere, since $p/p_{oo} \sim 1$, the particular choice of α does not ~~strongly~~ greatly affect the radiation budget. However, the radiation budget in the stratosphere may be very sensitive to the choice of α, since $p/p_{oo} \leq 0.1$. Consequently, if the pressure scaling approximation embodied in (II.3) is to be utilized for a GCM which includes the stratosphere, a careful selection of α is required.

A value of $\alpha = 1$ was adopted for the UCLA 2-layer moist ~~model~~ GMC. A value of $\alpha = 0.6$ is currently being used in ~~in use with~~ the UCLA 3-layer GCM. Preliminary results indicate that the difference ~~between~~ in the cooling rate of a tropospheric layer, for these two values of α, is about $0.1^{\circ}C$/day.

2. Effective amount of carbon dioxide

In the earth's atmosphere, the spatial and seasonal variation of carbon dioxide content is less than 2 per cent. Except for studies of the influence of CO_2 on climate, we can assume that the CO_2 in the atmosphere is constant in space and time. It is assumed in the following that the amount of CO_2 is 0.032 per cent by volume (320 ppm), that is 0.0489 per cent by weight.

Following Yamamoto (1952), the pressure scaling factor a for CO_2 is assumed to be 1.0. The effective amount of CO_2 from the earth's surface to a level p, which is usually expressed as a thickness at normal temperature (0°C) and pressure (1 atmosphere or 1000 mb), is given by dividing (II.3) by ρ_{NTP} as follows:

$$u^*_{CO_2}(p, p_s) = \frac{1}{g\rho_{NTP}} \int_{p}^{p_g} q_{CO_2} \frac{p}{p_{oo}} dp$$

$$= h(p_s^2 - p^2)/p_{oo}^2 \qquad \text{(IV.17)}$$

where

$$h = \frac{q_{CO_2} p_{oo}}{2g\rho_{NTP}} = 126 \text{ cm-NTP} \qquad \text{(IV.18)}$$

and q_{CO_2} is the percentage content of CO_2 by weight (0.0489%), ρ_{NTP} is the density of CO_2 at NTP (1.977×10^{-3} g cm^{-3}), p_s is the surface pressure and h is the total effective amount of CO_2 in an air column. The effective amount of CO_2 in the layer between p_i and p_j is then

$$u^*_{CO_2}(p_i, p_j) = 126 \frac{|p_i^2 - p_j^2|}{p_{oo}^2} \text{ cm-NTP} \,. \qquad \text{(IV.19)}$$

If the pressure scaling factor for carbon dioxide is α, the following general form is obtained instead of (IV.19):

$$u^*_{CO_2}(p_i, p_j) = \frac{2h'}{\alpha+1}\left|\left(\frac{p_i}{p_{oo}}\right)^{\alpha+1} - \left(\frac{p_j}{p_{oo}}\right)^{\alpha+1}\right| \qquad \text{(IV.20)}$$

where $h' = \rho_{CO_2} p_{oo} / 2g\rho_{NTP} = 0.126 \times (1000)^{\alpha}$ cm-NTP.

V. SUMMARY

Simplified schemes have been presented for calculating the short wave and long wave radiative heating of clear and cloudy air, which can be used in numerical general circulation models with a coarse vertical resolution.

(i) Long wave radiation

(a) A bulk transmission function was introduced and its value was determined by interpolation between 1.0 and the transmission function of the layer. The interpolation factors were parameterized as a function of the thickness of the layer, the pressure, the water vapor mixing ratio at a reference level, and the lapse rates of the temperature and mixing ratio of the layer. The interpolation factor is linearly proportional to the thickness of the layer and varies slightly with the pressure and mixing ratio at the reference level. The effect of the lapse rates of temperature and mixing ratio is relatively small and is negligible in many cases.

(b) It was assumed that any cloud occurring in a layer with a temperature less than -40°C allows transmission of a fraction of the incident long wave radiation. This effect was roughly approximated by reducing the cloud amount by the transmissivity of the cloud.

(c) Empirical expressions for the transmission functions of water vapor and carbon dioxide were presented and the errors of the expressions were tabulated.

(d) For simplicity, a pressure scaling approximation was adopted for the radiation computation. Scaling factors of either 0.6 or 1.0 for water vapor, and 1.0 for carbon dioxide, were employed. Test calculations showed that the radiation budget in the troposphere was not sensitive to the choice of the value of the scaling factor.

(ii) Solar radiation

(a) The solar spectrum was divided into ~~the parts, the~~ a scattered part and ~~the~~ an absorbed part. The scattered part, with wavelength less than 0.9μ, undergoes conservative Rayleigh scattering ~~but its~~ with no absorption by water vapor ~~is negligible~~. The absorbed part, with wavelengths larger than 0.9 μ, undergoes absorption with ~~negligible~~ no Rayleigh scattering. This ~~concept~~ approximation significantly simplifies the solar radiation calculation for a clear sky.

(b) A cloud layer was regarded as a fictitious layer of water vapor that absorbs the same amount of solar insolation as the cloud layer. This concept considerably simplifies the solar radiation calculation for ~~the~~ an atmosphere with clouds. The ~~values~~ average of the equivalent cloud water vapor amount were estimated for four typical cloud types ~~under normal conditions~~.

(c) General schemes for ~~the~~ estimation of the absorption of solar radiation in an atmospheric layer, and at the earth's surface, were presented for ~~the cases of~~ 1) a clear sky, 2) a quasi-vertical single cloud layer, and 3) quasi-horizontal multiple cloud layers.

(iii) Vertical distribution of water vapor and carbon dioxide

~~(d) To obtain the effective water vapor and carbon dioxide amounts~~ For the radiation calculation, ~~it is necessary to know~~ the vertical distributions of the mixing ratios of water vapor and carbon dioxide must be known throughout the entire atmospheric column. It was assumed that the mixing ratio of water vapor in the stratosphere above 100 mb has the constant value of 2.5×10^{-6} g/g irrespective of season or latitude. Furthermore, it was assumed that the ~~percentage~~ amount of carbon dioxide by volume is 320 ppm throughout the ~~global~~ atmosphere. It was shown that the normal vertical profile of the water vapor mixing ratio in the troposphere is well expressed by p^k and ~~it was recommended~~ the suggestion was made that the predicted vertical profile of the water vapor mixing ratio ~~predicted by~~ in the GCM be adjusted to p^k for the radiation calculation.

Acknowledgments

The author wishes to express his gratitude to Professors Y. Mintz and A. Arakawa for their valuable suggestions and continuous support of this work, and to Messrs. M. Schlesinger and H. Giroux who read the manuscript and offered helpful comments. He also wishes to thank the staff members of the Forecast Research Laboratory, of the Japan Meteorological Research Institute for their continuous encouragement. He is indebted to Mrs. H. Shinoda and Mr. J. Stevens for drafting the illustrations and to Ms. S. Lovell for the typing.

This work was supported by the U.S. National Science Foundation, Atmospheric Sciences Section (Grant GA-1470); by the U.S. National Aeronautics and Space Administration, Institute for Space Studies, Goddard Space Flight Center (Grant NGR 05-007-328); and by the U.S.-Japan Cooperative Science Program (Grant GF-369); and by the Japan Society for the Promotion of Science (Grant 4R001).

References

Arakawa, A., A. Katayama and Y. Mintz, 1969: Numerical simulation of the general circulation of the atmosphere. Proc. WMO/IUGG Symposium on Numerical Prediction, Tokyo 1968, pp. IV-7 to IV-8-12.

Callendar, G. S., 1941: Infrared absorption by CO_2 with special reference to atmospheric radiation. Q. J. Roy. Met. Soc., 67, 263.

Clodman, J., 1957: Some statistical aspects of cirrus cloud. Mon. Wea. Rev., 85, 37-41.

Coulson, K. L., 1959: Radiative flux from the top of a Rayleigh atmosphere. Ph.D. Thesis, Dept. Met., UCLA, 176 pp.

Elsasser, W. M., 1942: Heat transfer by infrared radiation in the atmosphere. Harvard Meteorological Studies, No. 6, 107 pp.

Feigel'son, E. M., 1964: Light and Heat Radiation in Stratus Clouds. Academy of Science of USSR, Inst. Phys. of Atmosphere, Moskva, 245 pp. (Translated from Russian, Jerusalem, 1966).

Fritz, S. and J. S. Winston, 1962: Synoptic use of radiation measurement from satellite TIROS II. Mon. Wea. Rev., 90, 1-9.

Gates, W. L., E. S. Batten, A. B. Kahle and A. B. Nelson, 1971: A documentation of the Mintz-Arakawa 2-level atmospheric general circulation model. The Rand Corporation, Santa Monica, Calif., 408 pp. R-877-ARPA

Howard, J. N., D. L. Burch, and D. Williams, 1955: Near-infrared transmission through synthetic atmosphere.. Geophysical Research Papers. No. 40, Air Force Cambridge Research Center, 244 pp.

Joseph, J. H., 1966: Calculation of radiative heating in numerical general circulation models. Tech. Rep. No. 1, Numerical Simulation of Weather and Climate, Dept. Met., UCLA, 60 pp.

Katayama, A., 1966: On the radiation budget of the troposphere over the northern hemisphere (I). J. Met. Soc. Japan, SII, 44, 381-401.

McDonald, J. E., 1960: Direct absorption of solar radiation by atmospheric water vapor. J. Meteor., 17, 317-328.

Joseph, J. H., 1970: On the calculation of solar radiation fluxes in the troposphere. Solar Energy, 13, 251-261.

Manabe, S. and F. Möller, 1961: On the radiative equilibrium and heat balance of the atmosphere. Mon. Wea. Rev., 89, 503-532.

Mastenbrook, H. J., 1968: Water vapor distribution in the stratosphere and high troposphere. J. Atm. Sci., 25, 299-311.

Mügge, R. and F. Möller, 1932: Zun Berechnung von Strahlungsströmen and Temperaturänderungen in Atmosphären von Beliebigem Aufbau. Z. für Geophys., 8, 53-64.

McKinnon, D. and H. W. Morewood, 1970: Water vapor distribution in the lower stratosphere over North and South America. J. Atm. Sci., 27, 483-493.

Murgatroyd, R. J., P. Goldsmith and W. E. H. Hollings, 1955: Some recent measurements of humidity from aircraft up to height of about 50,000 ft. over southern England. Q. J. Roy. Met. Soc., 81, 533-537.

Orvig, S. (ed.), 1970: Climates of the polar region. World Survey of Climatology, V. 14., 370 pp.

Posey, J. W. and P. F. Clapp, 1964: Global distributions of normal surface albedo. Geophysica International, 4, 33-48.

Rodgers, C. D., 1967: The radiative heat budget of the troposphere and lower stratosphere. Planetary Circulation Project, Dept. Met., MIT, Rep. No. 2, 99 pp.

Smith, W. L., 1966: Note on the relationship between total precipitable water and surface dew point. J. App. Met., 5, 726-727.

Williamson, E. J., and J. T. Houghton, 1965: Radiometric measurements of emission from stratospheric water vapor. Q. J. Roy. Met. Soc., 91, 330-338.

Yamamoto, G., 1952: On a radiation chart. Sci. Rept. Tohoku Univ., S.5, Geophysics, 4, 9-23.

Yamamoto, G. and G. Onishi, 1948: Absorption coefficient of water vapor in the far infrared region. Sci. Rept. Tohoku Univ., S.5, Geophysics, 1, 71-75.

Appendix A: The finite difference scheme for long wave radiation for the 3-layer model

The general form of the finite difference analog for the flux of long wave radiation is given by (II.45). In the current UCLA 3-layer GCM, the cloud thickness is defined in a somewhat different manner from the general case. As shown in Fig. A-1, the lowest cloud is situated between levels 4 and 5. Assuming that $T_\infty = T_o$, we obtain

$$R_o = \sigma T_c^4 \tilde{\tau}_{\infty o} + \tau_{\infty o}\Delta B_{co} + \frac{1+m_o^+}{1+m_o^+}\tau_{2o}\Delta B_{o2}(1-CL_1') + \frac{\tau_{2o}+\tau_{4o}}{2}\Delta B_{24}(1-CL_1')(1-CL_3') + \left(\frac{\tau_{4o}+\tau_{6o}}{2}\Delta B_{46} + \tau_{6o}\Delta B_{6g}\right)(1-CL_1')(1-CL_3')(1-CL_5'),$$

$$R_2 = \left(\sigma T_c^4 \tilde{\tau}_{\infty 2} + \tau_{\infty 2}\Delta B_{co} + \frac{1+m_2^-}{1+m_2^-}\tau_{o2}\Delta B_{o2}\right)(1-CL_1') + \frac{1+m_2^+}{1+m_2^+}\tau_{42}\Delta B_{24}(1-CL_3') + \left(\frac{\tau_{42}+\tau_{62}}{2}\Delta B_{46} + \tau_{62}\Delta B_{6g}\right)(1-CL_3')(1-CL_5'),$$

$$R_4 = \left(\sigma T_c^4 \tilde{\tau}_{\infty 4} + \tau_{\infty 4}\Delta B_{co} + \frac{\tau_{o4}+\tau_{24}}{2}\right)(1-CL_1')(1-CL_3') + \frac{1+m_4^-}{1+m_4^-}\tau_{24}\Delta B_{24}(1-CL_3') + \left(\frac{1+m_4^+}{1+m_4^+}\tau_{64}\Delta B_{46} + \tau_{64}\Delta B_{6g}\right)(1-CL_5'),$$

($\frac{\tau_{o4}+\tau_{24}}{2}$ ... $\Delta B_{o,2}$)

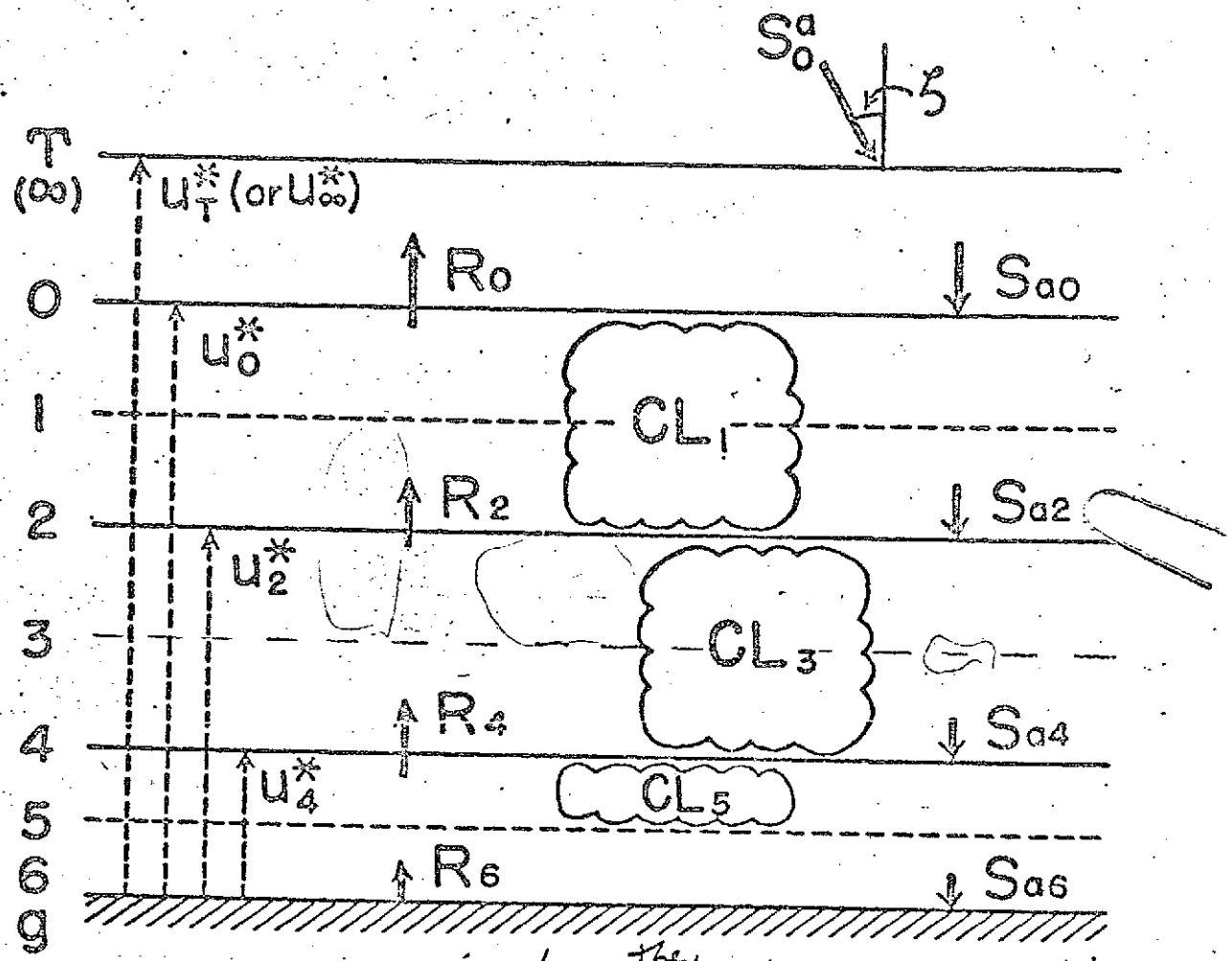

Fig. A-1. Schematic representation of the clouds and radiation fluxes in the ~~figure 10~~ 3-level general circulation model.

$$R_6 = \left(\sigma T_c^4 \tilde{\tau}_{\infty 6} + \tau_{\infty 6}\, \Delta B_{c0} + \frac{\tau_{06}+\tau_{26}}{2}\, \Delta B_{02}\right)(1-CL_1')(1-CL_3')(1-CL_5')$$
$$+ \frac{\tau_{26}+\tau_{46}}{2}\, \Delta B_{24}\,(1-CL_3')(1-CL_5') + \frac{1+m_6^-\tau_{46}}{1+m_6^-}\, \Delta B_{46}\,(1-CL_5')$$
$$+ \frac{1+m_{56}\tau_{56}}{1+m_{56}}\, \Delta B_{55}\, CL_5' + \Delta B_{6g} \quad .$$

where $$\Delta B_{ij} = \sigma T_i^4 - \sigma T_j^4 \quad ,$$

$$CL'_i = \alpha'_i CL_i \quad ,$$

and CL_i is the cloudiness and α'_i is the greyness of a cloud. If the temperature in a non-convective cloud layer is less than -40°C, $\alpha'_i = 0.5$ is assumed. The second term from the last in the expression for R_s is an additional term necessitated by the assumption that the bottom of the lowest cloud is level 5; m_{56} denotes the interpolation factor m for the layer between levels 5 and 6.

Appendix B: The finite difference scheme for solar radiation for the 3-layer model

In the following, the general expressions developed in section III.4 (ii) for the solar radiation calculation will be specialized to the present UCLA 3-layer GCM.

The cloudiness CL_i is restricted to either 0 or 1. Thus, if $\ell_i = 1$, $CL_i = 1$ and, if $\ell_i = 0$, $CL_i = 0$; therefore,

$$\ell_i = CL_i \quad . \tag{B.1}$$

In the following, CL_i will be substituted for ℓ_i everywhere.

Employing the relations

$$(1-CL_i)^2 = (1-CL_i) \quad ,$$

$$CL_i^2 = CL_i \quad ,$$

$$CL_i(1-CL_i) = 0 \quad ,$$

and the definition $CR_i = CL_i R_i$, we obtain from (III.45), (III.43), (III.37), (III.44) and (III.42):

$$w'(\ell_i) = w'(CL_i) = 1-CR_i \quad , \tag{B.2}$$

$$w(\ell_i) = 1 \quad ?$$

$$M_i = \prod_{i=1}^{i-3} (1-CL_i) \quad ? \tag{B.3}$$

$$W'(\ell_1, \ldots, \ell_n) = \prod_{i=1}^{n} (1-CR_i) \quad , \tag{B.4}$$

and

$$W(\ell_1, \ldots, \ell_n) = 1 \quad . \tag{B.5}$$

(i) Absorption in the atmosphere

Combining (III.38), (III.39) and (B.3), the optical path length of the layer between the top of the atmosphere and level i, D_{Ti}, is:

$$D_{T0} = (u_T^* - u_0^*)\sec\zeta \,, \tag{B.6}$$

$$D_{T2} = D_{T0} + (1-CL_1)(u_0^* - u_2^*)\sec\zeta + 1.66\, CL_1\, u_{c1}^* \,, \tag{B.7}$$

$$D_{T4} = D_{T2} + (1-CL_3)(u_2^* - u_4^*)[(1-CL_1)\sec\zeta + 1.66\, CL_1] + 1.66\, CL_3\, u_{c3}^* \,, \tag{B.8}$$

$$D_{T6} = D_{T4} + (1-CL_5)\, u_4^* \{(1-CL_1)(1-CL_3)\sec\zeta + 1.66[1-(1-CL_1)(1-CL_3)]\} + 1.66\, CL_5(u_{c5}^* + u_5^*) \tag{B.9}$$

where the last term on the right hand side of (B.9) is an additional term due to the assumption that the base of cloud 5 is level 5 as shown in Fig. A-1.

From (III.47) and (B.4), the downward flux at level i of the absorbed part of the solar radiation is

$$S_{ai} = S_o^a \left[\prod_{j=1}^{i-1} (1-CR_j)\right][1-A(D_{Ti})] \,. \tag{B.10}$$

Thus, for i = 0, 2, 4 and 6,

$$S_{a0} = S_o^a [1-A(D_{T0})] \,, \tag{B.11}$$

$$S_{a2} = S_o^a (1-CR_1)[1-A(D_{T2})] \,, \tag{B.12}$$

$$S_{a4} = S_o^a (1-CR_1)(1-CR_3)[1-A(D_{T4})] \,, \tag{B.13}$$

$$S_{a6} = S_o^a (1-CR_1)(1-CR_3)(1-CR_5)[1-A(D_{T6})] \,, \tag{B.14}$$

From (III.49), the absorption in the atmospheric layers j = 1, 3, 5 is

$$AS_1 = (1-CR_1)\, S_{a0} - S_{a2} \,, \tag{B.15}$$

$$AS_3 = (1-CR_3)\, S_{a2} - S_{a4} \,, \tag{B.16}$$

$$AS_5 = (1-CR_5)\, S_{a4} - S_{a6} \,. \tag{B.17}$$

(ii) Absorption by the earth's surface

Let $$CR_i = R(CL_i) = CL_i R_i \,, \tag{B.18}$$

$$CR_{ij} = R(CL_i, CL_j) \,, \tag{B.19}$$

$$CR_{ijk} = R(CL_i, CL_j, CL_k) \,. \tag{B.20}$$

Applying (III.46) to (III.13) and (III.14) yields

$$CR_{ij} = 1 - \frac{(1-CR_i)(1-CR_j)}{1-CR_iCR_j} \,, \tag{B.21}$$

and

$$CR_{135} = 1 - \frac{(1-CR_1)(1-CR_3)(1-CR_5)}{1-(CR_1CR_3+CR_3CR_5+CR_5CR_1)+2CR_1CR_3CR_5} \,, \tag{B.22}$$

$$= 1 - \frac{M}{2-M-(CR_1+CR_3+CR_5)+CR_1CR_3CR_5} \,,$$

where $M = (1-CR_1)(1-CR_3)(1-CR_5)$.

(a) The absorbed part

The absorbed part of the solar radiation that reaches the earth's surface can be obtained from (III.50) - (III.53). From (III.50) and (B.20),

$$S'_{as} = \frac{S^0_{as}}{(1-\alpha_s CR_{135})} \,. \tag{B.23}$$

From (III.51), (III.52) and (B.18) - (B.20), the contribution to the downward flux of solar radiation at the earth's surface from multiple reflections due to the top of cloud i+1, S^i_{as}, is

$$S^3_{as} = S_{a3}\, CR_3\, \frac{CR_1(1-CR_{35})}{(1-CR_1CR_{35})(1-\alpha_s CR_{135})} \,, \tag{B.24}$$

$$S^4_{as} = S_{a4}\, CR_5\, \frac{CR_{13}(1-CR_5)}{(1-CR_{13}CR_5)(1-\alpha_s CR_{135})} \,, \tag{B.25}$$

The total absorbed part of the solar radiation reaching the earth's surface is then by (III.53),

$$S'_{as} + S^2_{as} + S^4_{as} \quad , \tag{B.26}$$

(b) The scattered part

The scattered part of the solar radiation that reaches the earth's surface can be obtained from (III.54) and (III.55),

$$S_{s6} = \bar{S}_o \frac{1-\alpha_c}{1-\alpha_c \alpha_s} \quad , \tag{B.27}$$

$$\alpha_c = 1-(1-\alpha_o)(1-CR'_{13s}) \quad , \tag{B.28}$$

where CR'_{13s} is the total albedo of the clouds in the entire atmospheric column; CR'_{13s} is found by replacing CR_i by CR'_i in (B.22) and using $CR'_i = CL_i R'_i$ where R'_i is the albedo for the scattered part of cloud i.

Finally, the total downward flux at the earth's surface is $S'_{as} + S^2_{as} + S^4_{as} + S_{ss}$. Therefore, by (III.56), the absorption at the earth's surface is

$$S_6 = (1-\alpha_s)(S'_{as} + S^2_{as} + S^4_{as} + S_{ss}) \quad ,$$

$$= (1-\alpha_s)\left\{ \frac{1}{1-\alpha_s CR_{13s}} \left[S_{a3} + S_{a2} \frac{CR_3 CR_1 (1-CR_{35})}{1-CR_1 CR_{35}} \right.\right.$$

$$\left.\left. + S_{a4} \frac{CR_5 CR_{13} (1-CR_5)}{1-CR_{13} CR_5} \right] + S^s_o \frac{1-\alpha_c}{1-\alpha_c \alpha_s} \right\} . \tag{B.29}$$

In the actual programing, clouds are indexed somewhat differently from the present description. Cloud types 1, 2 and 3 refer to cloud layers 1, 3 and 5 of the present indexing scheme, respectively. The values of the equivalent cloud water vapor amount, u^*_{ci}, for cloud types 1, 2 and 3 are adopted for high, middle and low clouds, respectively, as shown in Table III-2. The surface albedos currently in use are presented in section III.5.

Appendix C: Required accuracy of m

For simplicity, consider the layer between levels i-2 and i shown in Fig. II-3. From (II.16) and (II.17), the contributions of this layer to the net flux of long wave radiation at levels i and i-2 are respectively

$$C_{i-1,i} = (\pi B_i - \pi B_{i-2})\bar{\tau}_{i-2,i} \quad)$$

and

$$C_{i-1,i-2} = (\pi B_i - \pi B_{i-2})\bar{\tau}_{i,i-2} \quad .$$

From (II.11), the fractional contribution of the above fluxes to the heating rate of the layer between i-2 and i, h, is

$$h = \frac{g(C_{i-1,i} - C_{i-1,i-2})}{c_p \Delta p} \quad .$$

Assuming a constant temperature lapse rate, $\Gamma = \partial T/\partial p$, h becomes

$$h \doteq 4g\, c_p^{-1} \sigma T_i^3 \Gamma(\bar{\tau}_{i-2,i} - \bar{\tau}_{i,i-2}) \quad ,$$

where the following approximation has been used

$$T_i^4 - T_{i-2}^4 \doteq 4T_i^3(T_i - T_{i-2}) = 4\Delta p\, \Gamma\, T_i^3 \quad .$$

If $\bar{\tau}$ has a maximum error of $(\Delta\bar{\tau})_{MAX}$, the error of h, Δh, is

$$\Delta h \lesssim 8g\, c_p^{-1} \sigma T_i^3 \Gamma (\Delta\bar{\tau})_{MAX} \quad .$$

The maximum possible value of Δh is then

$$(\Delta h)_{MAX} \doteq 8g\, c_p^{-1} \sigma T_i^3 \Gamma (\Delta\bar{\tau})_{MAX} \quad .$$

Considering somewhat large values of T_i and Γ, such as $T_i = 300^\circ K$ and $\Gamma = 8^\circ K/100$ mb, we find

$$(\Delta\bar{\tau})_{MAX} \doteq (\Delta h)_{MAX}/7.2 \quad , \qquad (C.1)$$

where the unit of Δh is $^\circ K\ day^{-1}$.

Now, we consider that a 10 per cent error is permissible in the ~~estimation~~ calculation of the heating rate. The maximum cooling rate of an atmospheric layer due to long wave radiation is about $2^{\circ}K\ day^{-1}$ in a clear sky. Then the maximum permissible error in the heating rate ~~may be~~ will be about $0.2^{\circ}K\ day^{-1}$. From (C.1), $\bar{\tau}$ is thus permitted to have a maximum error of about 0.03.

From (II.18) or (II.19), the error of the interpolation factor m is related to $\Delta\bar{\tau}$ as follows:

$$\Delta m = \frac{-\Delta\bar{\tau}\,(1+m)^3}{\Delta\bar{\tau}(1+m)+(1-\tau)} \qquad (C.2)$$

The maximum permissible error in m, for $\Delta\bar{\tau} = 0.03$, is shown in Table C-1 for several combinations of m and τ. The combinations shown in the Table above the heavy solid line occur in the real atmosphere only in extreme cases when Δp is larger than 100 mb. From this viewpoint, it is evident that the maximum permissible error in m is at least 20 per cent and increases with distance below the heavy solid line.

TABLE C.1. Required accuracy in m for the accuracy of 0.03 in $\bar{\tau}$.

m	τ								
	0.1	0.2	0.3	0.4	0.5	0.6	0.7	0.8	0.9
1	0.1	0.1	0.2	0.2	0.2	0.3	0.3	0.5	0.8
2	0.3	0.3	0.3	0.4	0.5	0.6	0.7	0.9	1.4
3	0.5	0.5	0.6	0.7	0.8	0.9	1.1	1.5	2.2
4	0.7	0.8	0.9	1.0	1.2	1.4	1.7	2.1	3.0
6	1.3	1.5	1.6	1.8	2.1	2.4	2.9	3.6	4.7
8	2.1	2.3	2.5	2.8	3.2	3.6	4.3	5.2	6.6
10	3.0	3.2	3.5	3.9	4.4	5.0	5.8	6.9	8.4
15	5.6	6.0	6.5	7.1	7.8	8.7	9.9	11.3	13.4

Appendix D: The seasonal variation of the sun's declination and distance from the earth.

In a numerical simulation of the seasonal variation of the general circulation of the atmosphere, the seasonal variation of the solar declination, δ, and the earth-sun distance, r_E, must be known.

The apparent orbital motion of the sun about the earth is shown in Fig. D-1 by the ellipse ABA'B'A with the earth located at focus F. The circle ACA'C'A represents the orbit of a fictitious sun which moves with constant speed and a one year period. Let the sun and fictitious sun be at perigee, A, at time t_o and at positions S and S' at time t, respectively.

The mean and true anomalies of the sun are shown by the angles M and ω. The mean anomaly is given by

$$M(t) = \frac{2\pi}{T} (t - t_o)$$

where T is the one year period. The date of perigee varies annually from Jan. 2 to Jan. 5. The mean date of perigee for the years 1950-1972 was Jan. 3.36 (UT). Thus, letting t represent the time in days from the beginning of a year, t_o is 2.36 days. Assuming T equal to 365 days, M is given by

$$M(t) = 0.0172142\ (t - 2.36), \text{ radians}$$

An asymptotic solution of Kepler's second law in terms of the eccentricity e of the elliptic orbit yields

$$r_E(t)/\bar{r}_E = A_o - A_1 \cos M - A_2 \cos 2M - A_3 \cos 3M - \ldots$$

and $$\omega(t) = M + B_1 \sin M + B_2 \sin 2M + B_3 \sin 3M + \ldots$$

where $$A_o = 1 + e^2 = 1.00027956$$

$$A_1 = e - \frac{3}{8}e^3 - \frac{5}{32}e^5 - \ldots \approx 0.01671825$$

$$A_2 = \frac{1}{2}e^2 - \frac{1}{3}e^4 - \ldots \approx 0.00013975$$

$$A_3 = \frac{3}{8}e^3 - \frac{135}{64}e^5 - \ldots \approx 0.00000175$$

$$B_1 = 2e - \frac{1}{4}e^3 + \frac{5}{96}e^5 - \ldots \approx 0.0334388$$

$$B_2 = \frac{5}{4}e^2 - \frac{11}{24}e^4 + \ldots \approx 0.0003494$$

$$B_3 = \frac{13}{12}e^3 - \frac{645}{940}e^5 + \ldots \approx 0.00000506$$

and $\bar{r}_E$ is one astronomical unit. The numerical values given above are for the earth's orbit ($e = 0.01672$).

Letting ℓ and ϵ denote the ecliptic longitude of the sun and the inclination of the earth's orbit ($23^\circ 27'$), respectively, the solar declination δ is given by

$$\delta(t) = \sin^{-1}(\sin \epsilon \sin \ell)$$

where $$\ell(t) = \omega(t) + \ell_o$$

and ℓ_o, the ecliptic longitude at perigee, is -1.3550737 radians (-77.64°). δ is positive for $0 \leq \ell \leq \pi$ and negative for $\pi \leq \ell \leq 2\pi$.